THESIS

ASSESSING HISTONE H2A.Z AND THE H2A TAILS IN CHROMATIN STRUCTURE

Submitted by

Erik Seidel

Department of Biochemistry and Molecular Biology

In partial fulfillment of the requirements

For the Degree of Master of Science

Colorado State University

Fort Collins, Colorado

Spring 2018

Master's Committee:

Advisor: Jeffrey Hansen

Laurie Stargell
Susan Bailey

ABSTRACT

ASSESSING HISTONE H2A.Z AND THE H2A TAILS IN CHROMATIN STRUCTURE

Deoxyribose nucleic acid (DNA) is a negatively charged macromolecule that encodes life's genetic material. In organisms, it is bound to net positively charged histone proteins in specific fashions and then compacts with magnesium and calcium to form domains and then chromosomes, which occupy territories in the nucleus during interphase. The mechanism of this compaction has been debated and studied for decades, and the employment of specific protein structures in molding chromatin morphology is still under review. This thesis adds to this story by testing how higher order chromatin structure is influenced by a histone H2A variant, H2A.Z, and the combined effect that the so-called histone H2A N and C terminal tails, when contrasted to arrays involving wildtype canonical H2A. An in vitro model system of nucleosomal arrays consisting of sea urchin derived 5S ribosomal DNA and recombinant mammalian histone proteins was used. Both the H2A.Z and H2A tailless arrays required increased magnesium to oligomerize into possibly domain-like structures. The H2A.Z protein produced similarly accessible structures as the fully accessible wildtype control as learned through a micrococcal nuclease digestion method designed for these chromatin structures. The deletion of the H2A N and C terminal tails produced oligomers with slightly less accessible linker DNA than its wildtype control according to the micrococcal nuclease digestion. Furthermore, the H2A.Z, H2A double tailless, and H2A wildtype oligomers were globular in shape. When subjected to fluorescence recovery after photobleaching (FRAP), the oligomers involving H2A.Z agreed with the current literature describing its presence in euchromatin and heterochromatin, and its mobility correlated with that of a more mobile and possibly more open structural agent. Taken together, the H2A and H2A.Z proteins are

influential in determining and providing variability to the overall chromatin structure that is vital to DNA's role in biology.

ACKNOWLEDGEMENTS

I acknowledge my family for their encouragement and for the traits they instilled in me that were necessary for me to even consider a master's degree, let alone in biochemistry.

I acknowledge my advisor, Dr. Jeff Hansen, who initially accepted me into his lab as a zoology graduate with essentially no lab experience and rudimentary biochemistry knowledge. This experience encouraged me46-147 to start a second bachelor's in biochemistry, and he then accepted me as a master's student. On a similar note, I want to acknowledge Dr. Ryan Rogge, who taught me most of the laboratory knowledge I have today, and for not giving up on me. Without Dr. Hansen and Dr. Rogge, I might have never entered scientific research, at least in biochemistry.

I want to thank my other committee members, Dr. Laurie Stargell and Dr. Susan Bailey, for their involvement on my thesis, thesis presentation, and defense.

Anyu Pan, an undergraduate biochemistry student, was also instrumental to my success, in supporting me, helping change buffers at inconvenient times for me or finishing started experiments, offering me tips, and consoling me when projects didn't work out. Charles "CJ" McDonald, the other master's student in the lab, and I willingly shared buffers, protocols, knowledge, and support, and I want to thank him for his help as we worked on very similar projects. CJ provided the wildtype histone octamers and the subsequent wildtype nucleosomal arrays experimented on in this thesis work, shown in figures 5 and 7. I worked with Mark Connolly and CJ McDonald on the FRAP data, FRAP data analysis, and fluorescent imaging. In addition to Mark, additional undergrads who I directly or indirectly worked with were Kyle Ray Anna Pryamkova, Julie Sanders, Kevin Nurzynski-Loth, Abigail McVay, Jordan Nelson, Lilia Maeda, and Thomas Martinez. I'm also grateful to the previous graduate students whose protocols, reagents, and the DNA that I ended up using.

I want to thank Dr. Hataichanok "Mam" Scherman of The Protein Expression and Purification Source for providing the individual purified histone proteins. The Peerson Lab allowed us to use their NanoDrop spectrometer, and the Santangelo Lab willingly allowed us to use their gel imager after our imaging computer failed. This research would not have been possible without the Biochemistry and Molecular Biology department (especially Neda Amidon, Dr. Eric Ross, and Nancy Reeves) as well as the College of Natural Sciences and Colorado State University. Dr. Barbara Bernstein, O'Neil Wiggan, Dr. Jeff Field, the Microscope Imaging Network, and the Markus and Stasevich labs helped with the fluoresce microscopy and fluorescence microscopy after photobleaching. I would also like to acknowledge anyone else who helped me but whose name I did not place here.

TABLE OF CONTENTS

LIST OF FIGURES

CHAPTER 1: BACKGROUND

Deoxyribonucleic acid (DNA) is a fundamental molecule to known life forms(*1, 2*). DNA's vital role in biology cannot be understated, since it was accepted that it encodes life's genetic material decades ago(*2*). Despite this, DNA's macromolecular structure and compaction mechanisms when bound with its fundamental histone proteins is only recently being exposed(*3*). Furthermore, recent research has increasingly begun to disprove the presence of a well-referenced structure that DNA and its associated histones was almost certainly thought to form in vivo (*4-7*). This thesis helps determine the role that specific histones play in histone bound DNA's macromolecular structure, which has potential wide-ranging implications for gene expression, DNA damage and repair, cell replication and development, genetic diseases, and the possibility of future personalized medicine.

1.1: Chromatin Structure

DNA has an overall negative charge thanks to its phosphate groups and is thus vulnerable to binding positively charged molecules. The basic histone proteins (*8*) are an option in Eukaryotes. The four canonical histones have remarkably similar structures and are highly conserved across species (*9*). From the N terminus to the C terminus, each histone consists of a N terminal tail, followed by a short alpha helix (alpha1), a short loop region (L1), a central longer alpha helix (alpha2), another short loop region (L2), another short alpha helix (alpha3), and finally a short (except in the case of H2A) C terminal tail (*8*). The region containing the three alpha helices as well as the two loops is labeled the histone fold (*8*). The N and C terminal tails are disordered when not bound and their structure thus their unbound structures cannot be determined by X-ray crystallography(*8*). The canonical histones are usually within the range of 11,000-15,000 daltons and approximately 102-135 amino acids long(*8, 10*).

The four canonical histone proteins associate with both DNA and with each other in a specific fashion. H2A and H2B establish a heterodimer, and two H3 and two H4 proteins produce a tetramer (*8*). An

octamer is formed when two dimers bind to a tetramer (*8*). This association process can be performed in vitro with high sodium chloride concentrations(*10*). It is the octamer that drapes 146-147 DNA base pairs around itself approximately 1.65 times (*8*). This structure is known as a nucleosome, and its crystal structure was published in 1997 (*8*). Nucleosomes are positioned along double-stranded DNA, and the region between each nucleosome is termed linker DNA(*11*). A series of nucleosomes is known as a nucleosomal array, which is also known as a 10nm fiber, as the nucleosome is approximately 6 by 11nm(*4, 11*). An illustration of the crystal structure of the nucleosome is found in part of **Figure 1.**

The 10nm fiber compresses the DNA 5-10 times(*12*). However, the 10nm fiber cannot be the only mechanism of compaction as it is estimated that two meters of DNA compacts into a single cell only microns in diameter (*13*). Furthermore, in vivo, chromatin exists in not only a relatively condensed heterochromatin state but also in a more open euchromatin state(*4*), expanding the level of compaction needed for less accessible regions. A debate continues to exist on how this compaction, known as higher-order chromatin structure, occurs, although recent studies have painted a clearer picture.

One method for describing further compaction was idealized to be the 30-nanometer structure, also known as folding, mediated in vitro through intra-array interactions(*11, 14*)This approximately 30nm long structure was mentioned in the 1980s and consisted of two main hypothesized structures- a one start helix (*15*) and a two-start helix (*16*). However, recent research is shedding doubt on the presence and importance of this structure in vivo. In one study, Small Angle X-Ray Scattering (SAXS) on isolated mitotic chromosomes produced a 30nm peak(*17*). However, subsequent analysis through cryo-EM determined that the responsible particles was not a 30nm chromatin structure but ribosomes whose 30nm peak disappeared after the ribosomes' removal(*17*). It was hypothesized that the 30nm chromatin structure forms under low (1-2mM) $MgCl_2$ concentrations as a result of nucleosome repulsion (*17*). A more recent paper on in vitro model constructed chromatin found no 30nm fibers under 4mM and 10mM $MgCl_2$ concentrations (*4*). This research instead found that 10nm fibers intrinsically formed

globular structures with a sedimentation coefficient of approximately 200,000 S that were 50-1000nm in diameter, without 30nm fibers (*4*). As the in vivo interphase nucleus combined magnesium and calcium concentration is approximately 6-10mM (*18*), it is unlikely that a 30nm structure that forms at ~1-2mM magnesium concentrations is of significant biological interphase significance. This finding(*4*) as well as previous work (*19*), suggests that the four canonical histones, DNA, and divalent cations ($MgCl_2$) together encodes the information necessary to produce a large, compact chromatin structure independent of the 30nm fiber(*4, 19*) .

There has been a recent increased effort to determine the higher order chromatin structure, independently of the 10nm fiber's role, through chromatin conformation capture (3c) and related techniques, focusing on topologically associated domains (TAD) (*20-23*). Chromatin within TADs has a greater likelihood of interacting with other molecules in its domain than with molecules from another TAD, and the included genes likely have similar gene regulation characteristics(*24*). Some have speculated that insulators and DNA binding proteins including transcription factors and CTCF play a role in TAD formation as reviewed in (*25*). However, a computer simulation study of Drosophila nucleosomal arrays found that that TAD formation was an inherent process of the arrays(*26*). Additionally, an in vitro study on reconstituted nucleosomal arrays also learned that nucleosomal arrays alone self-associated into in domain-sized globular oligomers (*4*), suggesting that factors beyond the histones and DNA themselves are not necessary for the elementary structure but can supply diversity for functional purposes (*3*). A summary figure of a view of chromatin structure is detailed in **Figure 1,** from a recent review paper published by the lab where this thesis was completed in (*3*). This model depicts that nucleosomal arrays form an interdigitated polymer melt structure that creates compact chromatin domains (*3*). These non-TAD domains are components of chromosomes, where each chromosome occupies its separate territory in the nucleus during interphase (*3*). However, the mechanisms of how the 10 nm fibers form these higher order structures remain a work in progress.

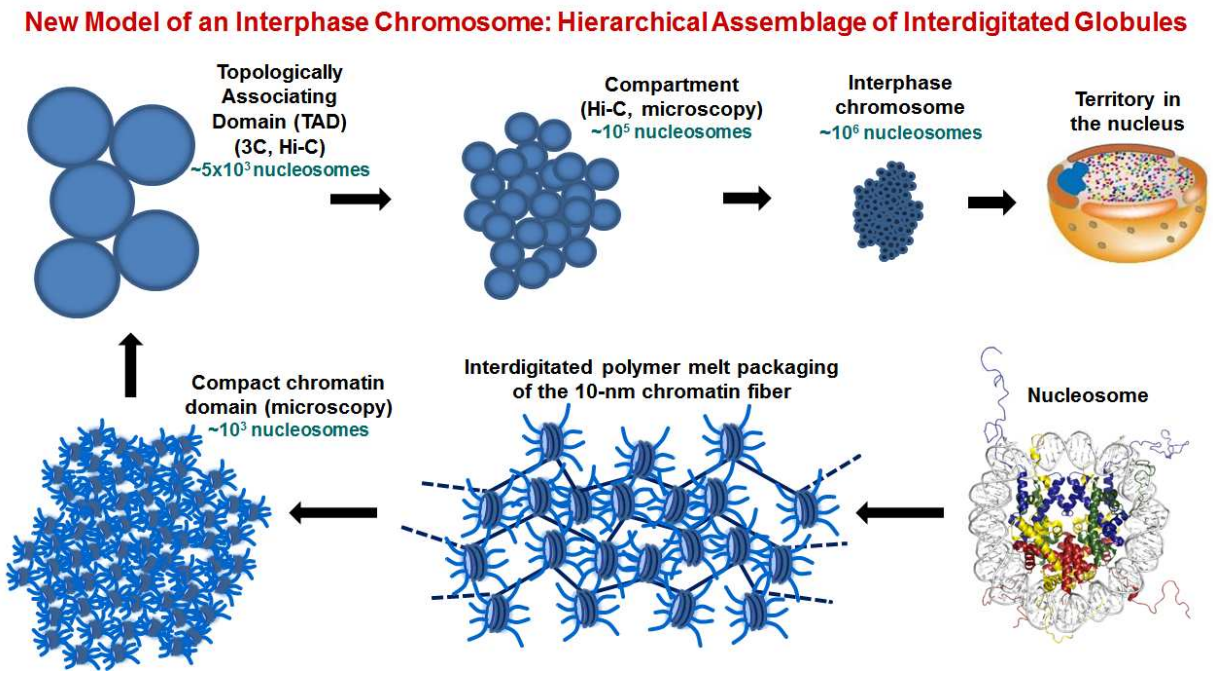

Figure 1: Nucleosomes to Chromosomes Model:
This figure, from a recent review paper from the lab where this thesis was completed(*3*) depicts an updated model of how 10 nm fibers (or nucleosomal arrays in vitro) compact into an interphase chromosome in the nucleus. A nucleosome is shown on the bottom right, with double stranded DNA wrapping around the two copies of the four canonical histone types. Adopted from Hansen, J. C., Connolly, M., McDonald, C. J., Pan, A., Pryamkova, A., Ray, K., Seidel, E., Tamura, S., Rogge, R., and Maeshima, K. (2017) The 10-nm chromatin fiber and its relationship to interphase chromosome organization, *Biochemical Society Transactions 5*, BST20170101.

1.2: Divalent Cations

It is documented that divalent cations, markedly calcium and magnesium, and to a lesser extent monovalent cations, play an important role in chromatin compaction(*14, 19*). A nucleosomal array will fold upon itself in intra-array interactions upon incubation with 1-2mM Mg, forming a 30nm fiber (*27*). More importantly, inter-nucleosomal array interactions are induced at $MgCl_2$ concentrations above 2mM(*19*). This nucleosomal array oligomerization, possibly equivalent to long-range interactions in vivo(*4*), is a rapid, reversible, histone tail mediated and not strictly coulombic process(*19*). In contrast, naked DNA does not undergo oligomerization(*19*). An in vitro study found that chromatin with canonical histones and the 601-12 DNA sequence first fully pelleted in a centrifuge sedimentation assay at approximately 4mM Mg, and that a further increase in magnesium concentration did not yield

significantly larger oligomers of strands of nucleosomal arrays (*4*). Each mole of calcium or magnesium can hypothetically bind to two moles of negatively charged phosphate groups on DNA(*28*). As a nucleosome has a net charge of approximately -148 and since each linker DNA base pair has a net charge of -2 (*29*), it is possible that this level of positively charged magnesium could further neutralize the remaining unmasked sites on DNA to increase the favorability of chromatin compaction. Not all of the negative phosphates need to be masked, however, as nucleosomal arrays have a net negative charge from 0-40mM $MgCl_2$ (*30*), and that an estimated 90% of naked DNA's phosphates necessitate neutralization to undergo the different process of condensation (*31*). As arrays do not oligomerize in monovalent salts (*19*) or when all histone N terminal tails are removed (*32*), the mechanism is not as simple as an electrostatic interaction. It is speculated that magnesium could also lead to DNA bending (*33, 34*). In vivo interphase nucleus concentrations are around 4-6mM for calcium, and 2-4mM for Mg, for an approximate total concentration of divalent cations relevant for chromatin oligomerization of 6-10mM (*18*). Although largely electrostatic, the precise mechanism of how magnesium and calcium induce chromatin compaction is not fully determined.

1.3: Histone Tails

Previous research has highlighted the importance of the core histone tails in determining chromatin structure. These tails are thought to promote compaction through both local and distant association mechanisms (*19, 35*), and that all of the canonical histone amino N terminal tails are involved in the process in an independent and additive fashion (*32*). It has been hypothesized that the basic histone tails, which account for nearly half of the histones' positive charges (*36*), shield negative charges on the DNA(*37*). The tails possibly also interact with protein regions themselves to induce chromatin compaction as reviewed (*38*), including on a negatively charged region contributed by H2A and H2B described as the acidic patch(*37*). Tails can also bind to chromatin accessory and other proteins,

and the tails can be modified by acetylation, methylation and by other post-translational modifications that can alter chromatin shape and provide epigenetic information as reviewed (*39*).

Two of these tail types are H2A's N and C terminal tails. The structure of histone H2A with its disordered tails is shown in **Figure 2**. These H2A tails were modeled to have less inter-nucleosome interactions than H3 and H4 in 1mM Mg or 150mM NaCl (*33*), and H2A N terminal tailless arrays required 3mM Mg to fully sediment in a centrifuge assay compared to 2mM Mg for wildtype, a lower difference than that of H3 and H4 tailless arrays (*32*). While this offers insight into how much magnesium is necessary for oligomerization, it does not elute information regarding the structure of the oligomerized macromolecules and how that compares to canonical H2A included nucleosomal arrays. Thus, using a double tailless mutant lacking both the N and C terminal tails should prove more impactful than a single tailless mutant, should be more insightful to the role that H2A's tails play in the compaction process as a whole, and could lead to future single tailless mutant experiments.

Despite previous findings limiting the role of the H2A tails compared to the H3 and H4 tails as mentioned in the prior paragraph, they were likely determined to be involved in inter-fiber interactions (*33*), and the C terminal tail is involved in interactions in compact chromatin according to a computational study (*37*). Furthermore, in less condensed conformations, a review paper highlighted the likelihood of N and C terminal tails associating with nucleosomal and linker DNA (*39*), and another study found a contact between the C terminal tail and linker DNA (*40*), with these binding patterns differing on salt concentrations and the presence or absence of linker histones (*33*) . The C terminal tail is less studied than the H2A N terminal tail in terms of higher-order chromatin structure, as both an in vitro (*32*) and a computational (*41*) N terminal tail paper did not investigate them. Constructs lacking the C terminal tail resulted in decreased nucleosome stability, increased mobility partially influenced on amino acid residues 115-122, slower cellular growth rate and increased stress, and decreased ISWI-dependent remodeling dependent on residues 115-122 in a human cell line (*42*). The C terminal tail's

affects on chromatin structure beyond that of the 10nm fiber, however, apparently remains unknown. This thesis attempts to shed light on the size, shape, and compactness of H2A double tailless mutant containing chromatin as well as its linker DNA accessibility and provider more insight into its relationship with magnesium-induced oligomerization.

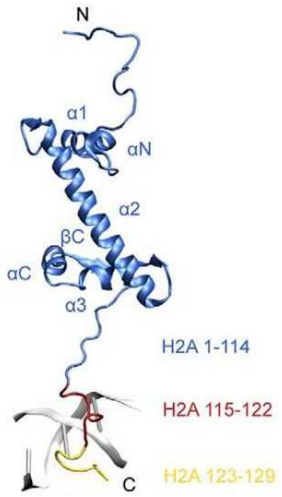

Figure 2: Histone H2A and its N and C Terminal Tails:
This figure, adopted from Histone H2A C-Terminus Regulates Chromatin Dynamics, Remodeling, and Histone H1 Binding (*42*), shows the histone H2A with an emphasis on its C-terminal tail. Adopted from Vogler, C., Huber, C., Waldmann, T., Ettig, R., Braun, L., Izzo, A., Daujat, S., Chassignet, I., Lopez Contreras, A. J., Fernandez-Capetillo, O., Dundr, M., Rippe, K., Langst, G., and Schneider, R. (2010) Histone H2A C-terminus regulates chromatin dynamics, remodeling, and histone H1 binding, *PLoS genetics 6*, e1001234.

1.4: Histone Variants and H2A.Z

Histones RNA transcripts beyond the H2A, H2B, H3, and H4 canonical histones can be translated at different cell cycle stages to replace predominately H2A and H3 in certain locations and durations (*43, 44*). Additionally, although separate from the histone variant class, linker histones, including histone H1, can bind to linker DNA and provide further compaction(*4*). Comparing a histone variant to the canonical version can provide insight into what effect the modified regions have on chromatin structure. Histone H2A variants maintain a relatively similar structure as the canonical H2A, including the 3 alpha helices in the histone fold and the N and C terminal tails, but can have in some cases dramatically different amino acid sequences(*43-45*). The highly conserved variant H2A.Z is of chromatin structural interest. Despite

only 60% primary structure similarity, H2A.Z's three dimensional structure is remarkably similar to that of H2A (*46*). The same is relatively true for a crystal structure of a H2A.Z replaced nucleosome with the exception of the dimer-tetramer and H2A or H2A.Z and H2B interactions, along with the acidic patch (*46*). The H2A.Z nucleosome crystal structure showed a weakened H2A.Z-H3 interaction compared to that of the H2A nucleosome, due to a glycine replacing a hydrogen bonding capable glutamine in H2A.Z's the C terminal docking domain (*46*). Another difference is a H2A.Z-H2A-Z alpha helix 1 alignment, which is parallel in the H2A-H2A interaction in the canonical nucleosome (*46*). Additionally, a hydrogen bonding rearrangement exists between the two dimers in the H2A.Z nucleosome crystal structure, and the H2A.Z-H2A.Z interaction is altered compared to that of the H2A nucleosome(*46*). However, the most intriguing difference in regards to chromatin structure is an extension of the acidic patch, where 6 amino acids are contributed by H2A and two by H2B (*46*). This negatively charged three-dimensional structure is extended in an H2A.Z nucleosome due to H2A.Z's negatively charged aspartate 97 and serine 98, the latter corresponding to a positive charge in H2A (*46*). The acidic patch is a binding site of both 9 residues of the H4 N terminal tail in addition to nucleosome binding proteins(*8, 47-49*). The H2A.Z nucleosome compared to the H2A nucleosome is depicted in **Figure 3**. A previous study

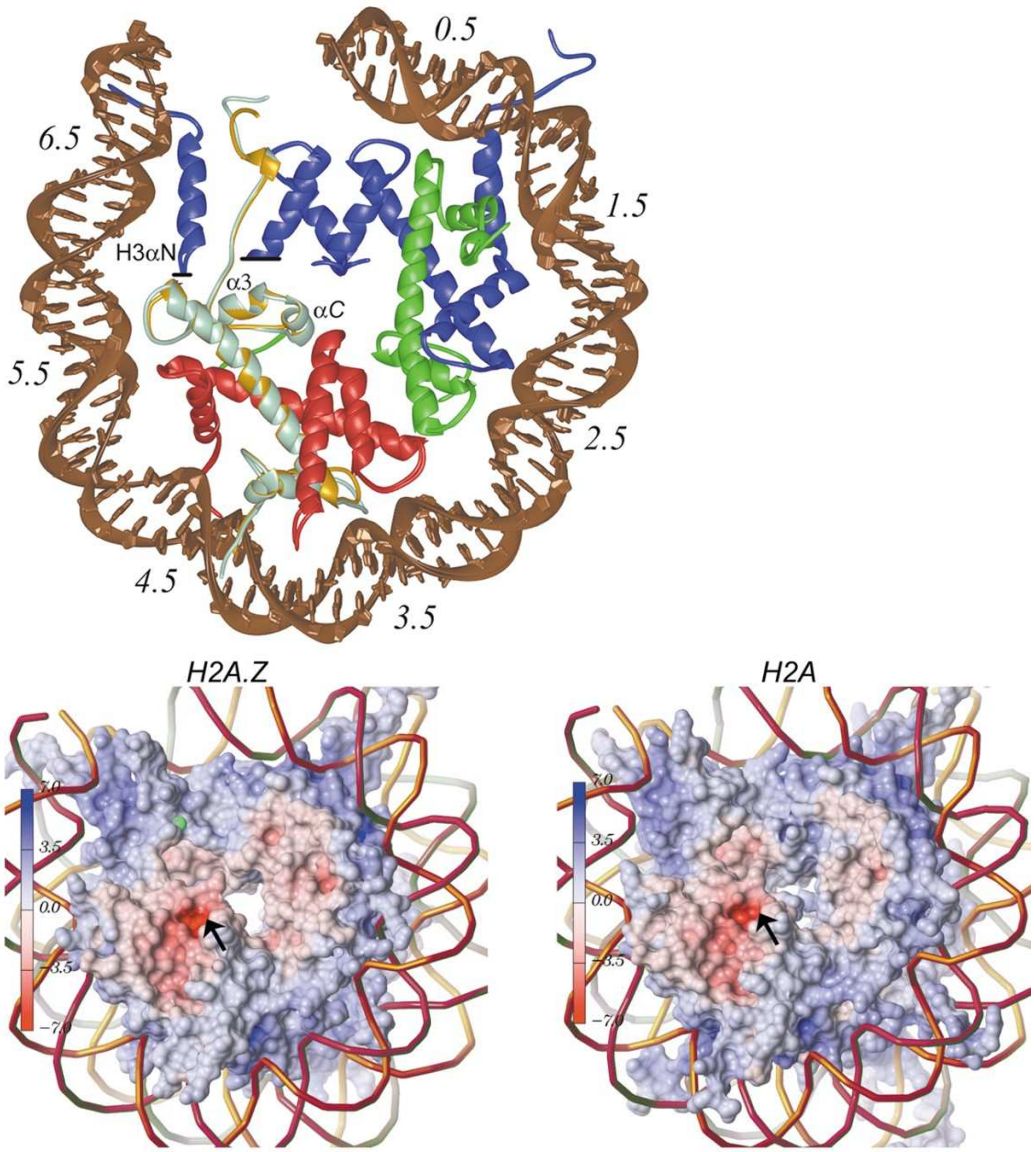

Figure 3: Comparing H2A.Z vs H2A Nucleosomes:
Top: Partial nucleosome with H2A.Z (gray) and H2A (yellow) superimposed on each other for comparing the two protein's paths(*46*). Bottom: Charge density maps of H2A.Z (left) and H2A (right) nucleosomes, with an arrow highlighting the acidic patch of each nucleosome(*46*). H2A.Z's acidic patch is extended by two base pairs(*46*). Adopted from Suto, R. K., Clarkson, M.J., Tremethick, D.J., and Luger, K. (2000) Crystal structure of a nucleosome core particle containing the variant histone H2A.Z, *Nature structural biology 7*, 1121-1124.

discovered that this acidic patch extension on H2A.Z lead to a larger sedimentation coefficient value and a more compact state at a low magnesium concentration of 1.5mM that was lost upon the mutation of these extended acidic patch residues to those residues found in H2A (*50*). This paper will further explore

this issue by assaying H2A.Z containing nucleosomal arrays at a fully compact magnesium state with that of biologically relevant divalent cation concentrations.

1.5: 208-12 DNA and Recombinant Histones Model System

Studying the effects of H2A.Z and the H2A tails in an in vivo study would need to account for the complexity and dynamic nature of the nucleus with transcription factors, polymerases, RNA transcripts and other artifacts, as well as cancer cell lines and also the complexity of knocking out histones that are necessary for survival(*51*). Thus, it would potentially be impossible to knock out histones or certain histone regions in vivo. Previous work has developed optimally binding nucleosome sequences of DNA, including the 208-12 and 601-12 sequences. The 208-12 sequence originated from a 5s ribosomal gene of the sea urchin Lytechinus variegatus (*52*), and has 12 208 base pair repeats for 12 optimal nucleosome binding sites (*53*), with an affinity several times stronger than in vivo genomic DNA (*54*). This 208 base pair repeat length is consistent with nucleus-isolated DNA from several experiments that found that nucleosomes were spaced every 160-210 base pairs(*55, 56*). In the 208-12 sequence, approximately half of nucleosomes on the related 207 base pair sequence were at positions 1-146, with the remainder of nucleosomes not starting at random positions but starting at a multiplier of 10 base pairs (*57*).

It was previously determined that these in vitro nucleosomal arrays form similarly sized oligomers to a structure found in vivo (topologically associated domains) (*4*). Additionally, SAXS experiments found that magnesium incubated reconstituted nucleosomal arrays had similar structures to those of magnesium incubated HeLa chromatin (*4*). Furthermore, increasing the concentration of the similar divalent cation calcium in vivo resulted in a more compact chromatin state (*58*), and that isolated nuclei is in line with the more oligomerized state resulting from increased magnesium concentrations previously done in the in the in vitro system (*4*) that this thesis utilizes. The 208-12 DNA sequence complexed with octamers used in this thesis was previously shown to have a sedimentation value of

around 29S, which is approximately equal to that of purified chicken erythrocyte 12 repeat octamer(*59*). Similarly, both the 208-12 sequence and this chicken-isolated sequence had a similar size-shape determined sedimentation coefficient of around 11S, and analytical ultracentrifugation experiments with varying NaCl concentrations produced similar sedimentation value curves on both array types (*59*). Thus, the system of using 208-12 DNA with recombinant histones is relevant to that of in vivo chromatin structures, with the benefit of testing homogenous histone mutants or variants.

1.6: Background on Methods Used

In this thesis, nucleosomal arrays were constructed with 208-12 DNA and canonical histone octamers, octamers where H2A.Z replaced H2A, and octamers where a double tailless H2A, residues 13-118, replaced the full length H2A. Several assays attempted to determine the structural characteristics of the H2A.Z and H2A tailless double arrays compared to the canonical H2A-H2B-H3-H4 based nucleosomal arrays.

1.7: Absorbance Sedimentation Velocity Analytical Ultracentrifugation

Several types of sedimentation velocity analytical ultracentrifugation (AUC) optics exist, including absorbance optics. This method depends on loading a reference solution and a sample solution into two separate chambers of an AUC cell apparatus with quartz (absorbance) windows (*60*). Absorbance AUC measures absorbance at a specified wavelength along radial positions (*60*). However, each scan takes approximately one minute, too short of a timeframe to obtain enough scans on saturated magnesium nucleosomal array samples for analysis at the lowest speed available of 3,000 rotations per minute on the AUC used in this thesis (*61*). Absorbance AUC is useful for testing pilot and bulk in vitro constructed nucleosomal array samples to ensure that each of the 12 octamer binding sites on a 208-12 DNA sequence is bound to an octamer, known as a saturated condition (*10*).

AUC is used to determine a sample's sedimentation coefficient, or S value. The S value is determined by the equation $\frac{M(1-v\rho)}{Nf}$, with M=mass of the object, v=an inverse density measurement,

N=Avogadro's number, and f=the frictional coefficient of the object(*60*). According this equation, an object with a larger mass will have a larger S value and will sediment faster. Further, a smaller frictional coefficient will produce a larger S value. Thus, if a spherical object and a rod have equivalent masses, the spherical object will have a smaller frictional coefficient than the rod and therefore will produce a larger S value and sediment faster. This means that larger, more condensed (less surface area) particles will produce larger S values and sediment faster. In the context of nucleosomal arrays, a larger S value translates to a larger complex with more arrays, a more compact structure, or a combination of a larger and more compact state.

In the context of testing for nucleosomal array saturation, it was previously determined that an S value of approximately 29S produced a molecular weight through approximately that of 12 octamers bound to 207-12 DNA, the molecular weight determined through a sedimentation equilibrium AUC run(*14*). The R value, or ratio of octamer moles per DNA repeat moles, has a linear relationship with the $\log(S_{50\%})$, the average S value of an S value distribution from an absorbance sedimentation velocity AUC run(*53*). Therefore, increasing octamer (histone) concentrations compared to DNA repeat concentration should lead to an increased S value, as this increases the mass of the nucleosomal array in the S value equation found in the above paragraph(*53, 60*). This makes the absorbance sedimentation velocity AUC a useful tool for determining nucleosomal array saturation levels to minimize this variable when comparing different array constructs.

1.8: Differential Centrifugation Assay

The differential centrifugation assay involves mixing an equal volume of arrays with differing concentrations of magnesium buffers, as described in previous work (*27*). After incubating on ice, the tubes are centrifuged for a set time. The supernatant is then measured on a NanoDrop spectrophotometer at 260nm absorbance. At low magnesium concentrations, very little of the sample pellets as the nucleosomal arrays interact with each other and with the cation to form less compact and

smaller structures. Increasing magnesium concentrations increase the amount of pelleting until essentially all of the chromatin sample pellets out of solution, leaving a supernatant absorbance near zero. The midway point of magnesium concentration where half of the sample is pelleted is known as the Mg50 point. The magnesium concentration where the sample is fully pelleted is then used for subsequent experiments. This assay also determines how much divalent cation is necessary for saturated chromatin and if a variant or mutant nucleosomal array sample more or less readily self-associates compared to the canonical arrays.

1.9: Micrococcal Nuclease Assay

The micrococcal nuclease assay sheds light on how accessible a chromatin's linker DNA strands are. This experiment uses the micrococcal nuclease enzyme, a calcium-dependent, non-specific but AT preference exo- and endonuclease protein that digests double stranded DNA (*56, 62-64*). Linker DNA is more susceptible to micrococcal nuclease digestion than DNA bound to nucleosomes, and thus linker DNA is digested first(*65*). Since nucleosomal DNA is relatively protected, and as nucleosomes are regularly positioned along the course of a 208-12 DNA strand, micrococcal nuclease digestion will result in a discrete banding pattern when the resultant DNA fragments are run on a gel (*64*). In order to obtain these DNA fragments, the DNA is removed of histones via a phenol-chloroform-isoamyl alcohol wash, and successively isopropanol precipitated to rid the DNA of phenol. Without any digestion, a single band at approximately 2500 base pairs appears, equivalent to the length of the 208-12 DNA strand. At earlier time points, the nuclease has not fully digested the linker DNA, leading to bands of various but relatively predictable lengths on a gel. Increased digestion time results in a higher concentration of shorter DNA bands of similar lengths. Complete digestion of linker DNA leads to a single band, and further time could eventually cause breakdown of the histone guarded DNA as well (*65*). The wildtype H2A array digestion pattern with several time points is then compared to the H2A.Z or H2A double tailless array in the

context of digestion rates, where a faster digestion rate for an array type presumably translates to more accessible linker DNA.

1.10: Fluorescence Imaging and Fluorescence Recovery After Photobleaching (FRAP)

Another useful assay for chromatin structure determination is fluorescent microscopy and fluorescent recover after photobleaching (FRAP). Fluorescent microscopy takes advantage of a fluorescent molecule's, such as SYBR Green 1's, ability to be energetically excited by photon absorption, relax to a lower increased energy state, and then fluoresce, or emit the photon at an increased wavelength to return to its ground energy state(*66*). SYBR Green 1 is a minor-groove primarily double stranded DNA intercalating agent with a preference for A-T base pairs (*67*). This aromatic compound's fluorescence increases at least 1000 times after binding with 3-4 DNA base pairs through intercalation and electrostatic interactions (*68*). In FRAP, a fluorescent confocal microscope equipped with a laser is used to bleach a specified chromatin structure on a microscope slide at a wavelength near the fluorophore's maximum absorption level(*66*). This bleaching results in a covalent alteration or destruction of the fluorophore, partially through the production of reactive oxygen species that causes the bleached region to lose its fluorescence capability(*66*). Although the bleaching is irreversible, neighboring unbleached fluorescently tagged DNA molecules diffuse into the bleached target, and the bleached molecules are also able to diffuse outwards, in what is known as the mobile fraction(*66*). This results in a recovery after photobleaching where the fluorescent intensity recovers to a certain percentage of what the fluorescence intensity was prior to the photobleaching(*66*). The percentage of unrecovered photobleaching is a result of the immobile fraction, due to photobleached DNA molecules that did not diffuse away from the photobleached spot(*66*). A half-life can also be quantified to determine the time necessary for the bleached area to recover 50% of its plateau post-bleach maximum fluorescence intensity(*66*). FRAP is useful for determining the mobility, or diffusion, of a fluorescently targeted object. In this case it is the DNA portion of nucleosomal arrays. It has been argued that if the

nucleosomal array 10nm fiber is the building block of higher order globular chromatin structures (*4*), and if the intrinsically disordered histone tails are valuable in higher-order chromatin structure, then chromatin has liquid-like properties and is thus mobile in vivo (*69, 70*). Thus, FRAP has the potential to inform about the different diffusion dependent mobility of the DNA portion of different chromatin samples and also potentially regarding chromatin accessibility. In addition to FRAP, simply imaging SYBR Green 1 tagged nucleosome bound DNA with a confocal fluorescent microscope presents an idea of the chromatin's overall shape and size.

1.11: Hypotheses

It was hypothesized that H2A.Z would orchestrate a more compact oligomerized nucleosomal array structure. According to this, H2A.Z arrays were hypothesized to oligomerize at a lower magnesium concentration the wildtype counterparts to oligomerize based on the differential centrifugation assay. H2A.Z oligomers were accordingly thought to have a faster micrococcal nuclease digestion rate. In comparison to the wildtype oligomers, H2A.Z oligomers were thought to produce an increased mobile fraction recovering at a faster rate based on the Fluorescence Recovery After Photobleaching (FRAP) results in light of the acidic patch mutant results based on arrays with neutralized acidic patches.

In contrast to the H2A.Z array predictions, the H2A tailless nucleosomal array constructs were predicted to have a more open structure as the tails were predicted to contribute to a more compact oligomer. Therefore, compared to their wildtype counterparts, H2A tailless constructs were predicted to require increased magnesium to oligomerize in the differential centrifugation assay, digest at a faster rate by the micrococcal nuclease enzyme, and have an increased Fluorescence Recovery After Photobleaching (FRAP) mobile fraction recovering at a faster rate.

1.12: Introduction to Thesis

In this work, histone octamers composed off two duplicates of H2A, H2B, H3, and H4, and 208-12 DNA, were combined into nucleosomal arrays. This sample is known as the wildtype arrays. In a

second array type, two copies of histone H2A, amino acid sequence 13-118 with the N and C terminal tails removed, replaced the two H2A copies. This sample is known as the H2A tailless or H2A globular arrays. In a third sample, two copies of the histone variant H2A.Z replaced the two copies of H2A, whose sample is labeled onwards as the H2A.Z arrays.

The H2A.Z and H2A tailless arrays were compared to the wildtype arrays through a micrococcal nuclease digestion, a centrifugation assay known as differential centrifugation, and fluorescence recovery after photobleaching (FRAP) and fluorescence microscopy. These studies attempted to determine the role that the H2A tails and the H2A.Z variant have on nucleosomal array oligomerization structure, including the size, shape, linker DNA accessibility, intrinsic mobility, and the amount of magnesium needed for oligomerization.

CHAPTER 2: METHODS

2.1 Histone Octamer Prep

The preparation of both H2A.Z and H2A double tailless octamers followed that of the lab's protocol, where further information regarding this is summarized in *Assembly of Nucleosomal Arrays from Recombinant Core Histones and Nucleosome Positioning DNA(10)*. Individual histones H2B, H3, and H4, and either H2A, H2A.Z, or tailless H2A with amino acids 13-118, were obtained from Colorado State University's Protein Expression and Purification Facility. The histones were denatured through an unfolding buffer of 6M guanidinium HCL, 20mM 7.5 pH Tris, and 5mM DTT at room temperature for 80 minutes(*10*). The histones were measured at 276nm on a NanoDrop spectrometer(*10*). They were then dialyzed with 6,000-8,000 molecular weight cutoff tubing in a refolding buffer consisting of 2M NaCl, 10mM ph7.5 Tris, 1mM EDTA, and 5mM beta-mercaptoethanol at 4 C°, with buffer changes after ~6 hours and ~12 hours(*10*) . Equal molar amounts of H3 and H4 were used, as well as equal molar amounts of H2B and either H2A, H2A.Z, or tailless H2A(*10*). However, 10% more of the H2B/H2A or H2A deviation was used than of H3/H4 to ensure for more precise FPLC octamer elution as the tetramer elutes at a similar volume as the octamer. The octamer was then purified from aggregates, tetramers, and dimers through Fast Protein Liquid Chromatography (FPLC) on a Superdex 200 (16/60) column(*10*). Absorbance was measured at 280nm(*10*). Fractions of interest were run on a 20% polyacrylamide gel to determine the fractions whose four histones were of relatively equal molar amounts(*10*). These fractions were then pooled and concentrated with an Ultra-15 centrifugal filter by Amicon with a molecular weight cutoff of 30,000 molecular and measured at a wavelength of 205 nm on a spectrometer(*10*). They were then checked on another 20% polyacrylamide SDS-PAGE gel before being used in nucleosomal array construction.

2.2: DNA Amplification and Purification

The DNA used here, 208-12 DNA, was cultured in E. coli and subsequently purified by a previous lab member. Pure 601-12 DNA was cloned in E. coli and purified to minimal success by the author and the lab as a whole.

2.3: Nucleosomal Array Reconstitution

Nucleosomal array reconstitution followed that of the lab's protocol, where further information regarding this can be found in *Assembly of Nucleosomal Arrays from Recombinant Core Histones and Nucleosome Positioning DNA(10)*. First, nucleosomal array pilots at molar ratios of octamer to 208-12 DNA repeats of 0.9, 1, and 1.1 were constructed(*10*). Twelve-to-fourteen thousand molecular weight cutoff dialysis tubing was used(*10*). Pilots were dialyzed in 2 liter buffers at 4 C° containing 10mM Tris pH 7.8, 1mM EDTA, and 1mM DTT for the first three buffers(*10*). In the fourth buffer, 0.1 mM PMSF was used(*10*). Buffers had subsequently lower sodium chloride concentrations, starting with 1 M NaCl, then 0.75 M NaCl, and then 0.75mM NaCl for the third and fourth buffers(*10*). Pilot nucleosomal array samples were run on an analytical ultracentrifuge using interference optics to determine the sedimentation coefficients to identify nucleosome per DNA nucleosome binding site saturation levels(*10*). It was previously shown that a sedimentation (S) value of around 29 correlated with ~12 nucleosomes per nucleosome binding site on a 208-12 DNA template (*71*). The bulk samples for wildtype, H2A.Z, and H2A tailless arrays were then constructed with the same method as the pilots, with the same mole of histone octamer to mole of DNA binding site as the pilot that had the closest S value to 29(*10*).

2.4: Differential Centrifugation Assay

An equal volume of nucleosomal arrays of wildtype, H2A.Z, or tailless, and of 2x magnesium buffer of a desired final magnesium concentration, was pipetted into a 1.5ml tube. For H2A.Z and wildtype arrays, the volume was 25ul for 6.25 ug of arrays measured by DNA amount, and for H2A tailless arrays, it was

14.88ul or 2.5ug of arrays. One replicate of the wildtype arrays also used 2.5ug instead of 6.25ug of arrays as measured by DNA quantity. The mixture was incubated on ice at room temperature for 5 minutes. The samples were then spun at 16,000 g for 5 minutes at 4 C° on a Hermle Z 233 MK-2 Labnet counter centrifuge. Then 2ul was removed from the supernatant and measured at 260nm absorbance that was blanked with 2ul of the 2x magnesium buffer diluted in half with array dialysis buffer 4. Three absorbance measurements were taken from each sample and averaged. Each replicate was divided by the 0mM Mg absorbance measurement to obtain the fraction of arrays remaining in the supernatant. Thus, the 0mM Mg had a fraction of 1.

2.5: Micrococcal Nuclease Experiments

Micrococcal nuclease experiments were performed for wildtype H2A, H2A.Z, and H2A double tailless nucleosomal arrays. For wildtype and H2A.Z arrays, 13ug or fifty-two microliters of 0.25 ug/ul arrays were combined with 169.89ul of 7mM 2x $MgCl_2$, 41.51ul of 0.75 mM stock calcium chloride, 76.83ul of Array Dialysis Buffer 4 composed of 10mM pH 7.8 Tris buffer, 0.25mM EDTA, 2.5mM sodium chloride, and 1mM PMSF, and 1.11ul of filtered water. For H2A tailless arrays, 13ug of arrays was also used, but this required 77.38 ul of array volume at 0.168 ug/ul, thus lowering the amount of array dialysis buffer 4 from 76.83ul to 51.45ul. The volume of 0.75 mM $CaCl_2$, 7mM 2x $MgCl_2$ buffer, and water amounts were the same as that of the wildtype and H2A.Z arrays. The method for all three array types was as identical as possible from this point forward. The arrays were then incubated in these ingredients on ice at room temperature for 15 minutes. After 15 minutes, 85ul of this mixture was removed. For all time points, including the time zero, eighty-five microliters were added and subsequently pipette mixed to a labeled 1.5ml epi tube, on ice, containing 9ul of 2.0mM EGTA pH 8.5, and 3.1ul of 450mM EDTA. The final EGTA concentration with the 85ul of arrays was 0.185mM and the final EDTA concentration was 14.367mM. This was the time zero measurement. After mixing, 0.219 ul of 1.667 units/ul Micrococcal nuclease enzyme was added to this mixture containing EDTA and EGTA and was placed on

ice. Then 0.3713ul of 7mM $MgCl_2$ 2x buffer was added to the bulk solution to keep the final Mg concentration at 7.0 mM, accounting for EDTA's chelation of magnesium at a 1:1 ratio. Then 0.658 ul of 1.667 units/ul micrococcal nuclease enzyme (in 10mM Tris, 50mM NaCl, 1mM EDTA, 50% glycerol, at pH 7.5 stored at -4 C°) was added to the bulk digest. The enzyme activity level was 0.1125 units of enzyme / ug of DNA. The digest was placed in a 37 C° water bath and was pipette mixed. For each incubation time point of 1.5, 3.5, and 8 minutes, 85 ul of this mixture was added to an EDTA/EGTA mix mimicking that of the 0 time point and pipette mixed and placed in an ice bucket at room temperature.

After the last time point was taken, 97.1ul, an equal volume to the finished digests, of a 25:24:1 ratio of phenol: chloroform: isoamyl alcohol was added. This was to remove the histone proteins and the micrococcal nuclease enzyme from the mixture. Each tube was vortexed for 70 seconds, and then all digest tubes were spun for 10 minutes at 20 C° with 22,000 g at on a Hermlie LabNet counter centrifuge. Then approximately 97.1 ul of the aqueous top layer was removed and placed into new 1.5ml epis. Then 24.25ul of 2.83M 5.2pH sodium acetate was added (0.25 volumes), with 121.25 ul of isopropanol (1 volume), for a final sodium acetate concentration of 0.283 M and 0.1 volumes. The digest products were then briefly vortexed, spun down on a tabletop centrifuge, and placed in a -20 C° freezer overnight.

The subsequent day, 2ul of 0.1 ug/ul glycogen was added, and the tubes were spun down for 45 minutes at 22,000 g at 4C. One hundred fifty microliters were removed and discarded before they were spun down again, for 35minutes at 22,000 g at 4 C°. Then nearly all of the remaining isopropanol/sodium acetate volume was removed. One hundred fifty microliters of -20 C° 70% ethanol was added to each digest, and the tubes were vortexed for 10 seconds, spun on a tabletop centrifuge for 30 seconds, and placed in a -20 C° freezer for 10 minutes. They were then spun for 40 minutes at 22,000 g at 4 C°. Seventy-five microliters were removed before being spun for 35 minutes at 22,000 g at 4 C°. Finally, the remainder of the predominately ethanol liquid layer was pipetted off. The pellets were

then dried for five minutes at room temperature, before 10ul of TE buffer (10mM pH 7.8 Tris, 1mM EDTA) was added and pipette mixed to dissolve the pellets.

Two microliters of 6x loading dye (orange, Fermentas brand) was added, and all 12ul was loaded onto a 2% agarose, 12 lane agarose gel. Four and a quarter microliters of 1kb ladder were added to the first lane. The gel ran at 83 volts, and was stained with ethidium bromide for 15 minutes, de-stained with TAE buffer for 15 minutes, and was imaged with UV light.

The naked DNA digestion was performed in the same fashion but used one-fifth the ratio of units of micrococcal nuclease per ug of DNA as with the arrays, at 0.0225 units of enzyme/ug DNA. However, the incubation mixture consisted of 2.045ul of DNA, 10.377 ul $CaCl_2$ (.908mM final), 30.158ul array dialysis buffer 4, 42.197 ul 7mM $MgCl_2$, and 0.553 ul water. Then 0.1315ul of 7mM 2x $MgCl_2$ was added to maintain an effective (non EDTA chelated) magnesium concentration of 7 molar, along with 0.234 ul of 0.625 units/ul of micrococcal nuclease enzyme. This enzyme activity was $1/5^{th}$ the amount of that used for the nucleosomal arrays. This was placed at 37 C° for the respective time points, 8 minutes. The remainder of the protocol was as similar to each of the other digests as possible.

The micrococcal nuclease gel banding intensities were measured through (Fiji Is Just) ImageJ software. For each micrococcal nuclease representative gel, the intensity of the top band of each array type at each time point where the band was present was divided by the top band's intensity of the 0 minute digestion time point for that representative gel, which was then averaged across the three representative gels. One-tenth of the amount of DNA of the 0 minute digest was loaded onto the gels compared to the amount of loaded DNA for the other time points, and thus each 0 minute time point's band intensity was multiplied by ten to correct for this. For the H2A.Z oligomer and its respective wildtype oligomer control, the full-length DNA band's intensity was not measurable at the last digestion time point (at 8 or 10 minutes) and thus was not used in the analysis. On a similar note, the last band in the H2A tailless digest representative gel on the right side in **Figure 17** was not used as well due to a low

overall intensity. The top band represents an undigested 208-12 DNA sequence, corresponding to a nucleosomal array pre-phenol wash. The intensities were then graphed and fitted to an exponential function.

2.6: Fluorescence Recovery After Photobleaching (FRAP) and Imaging

Five-millimeter round coverslips were run in a plasma cleaner at 15 PSI. Afterwards, the coverslips were soaked in 0.1 mg/ml poly-L-lysine and were incubated overnight in a dark setting. On the morning of imaging, the poly-L-lysine was removed via pipette and the coverslips were soaked in filtered water for six five-minute incubations to remove the excess poly-L-lysine.

Two microliters, or 0.5ug at 0.25ug/ul, of wildtype or H2A.Z arrays was mixed with 248 ul of array dialysis buffer 4 (10mM Tris at pH 7.5, 2.5mM sodium chloride, 0.25mM EDTA, and 1mM PMSF) and was spun at 7,000 g for 15 minutes at 4C in a tabletop centrifuge to remove already formed aggregates. For H2A tailless arrays, this spin down procedure was identical to that of the wildtype and H2A.Z arrays but to use 0.5ug of tailless arrays, it required 2.976ul of arrays and 247.024ul of array dialysis buffer 4. Then 250ul of a 6mM 2X $MgCl_2$ buffer was added for H2A.Z and wildtype arrays FRAP, and 7mM for the H2A tailless images. For the 0mM controls, 250ul array dialysis buffer 4 was added instead of 2x magnesium buffer. This mixture was then incubated on ice at room temperature for 30 minutes. After 30 minutes, this mixture was added to a new 1.5 ml tube with a 3D printed insert with a poly-L-lysine coated and freshly water incubated coverslip. This tube was then spun at 7,000 g for 15 minutes at 4 C° for the formed oligomers to pellet. Afterwards, the liquid was removed and the coverslip was incubated in a 5 ul SYBR Green 1 mixture, consisting of a 4 ul water and 1ul SYBR Green 1, for 30 seconds. After 30 seconds, the SYBR Green 1 was removed via pipette and 10 ul of Sigma mounting medium was added to the coverslip. The coverslip was then mounted to the microscope slide. After a five-minute incubation in mounting medium, excess mounting medium was removed from the slide and the coverslip was secured on the slide with green nail polish. The nail polish was allowed to dry 2-3

hours before the coverslip was dabbed with ethanol to remove a number four to signify the top of the coverslip.

The slides were imaged the same day as the sample slide preparation on an Olympus IX81 Inverted Spinning Disk microscope at Colorado State University's Fluorescence Microscopy/Image Analysis Center with SlideBook software. For FRAP, the settings included a wavelength of 488nm and 200 time points at 100 millisecond intervals. At least 3 photobleaching repetitions were performed on each slide. The slides were corrected for background intensity and for photobleaching.

CHAPTER 3: RESULTS

3.1: Nucleosomal Array Reconstitution

Octamers were made where two copies of mouse H2A.Z replaced both copies of mouse H2A. A separate batch of octamer was made with human H2A residues 13-118 replacing the mouse H2A proteins. The sequence of the wildtype mouse H2A and the double tailless human H2A is found in **Figure 4.** The canonical wildtype octamer and subsequent incorporation into arrays of mouse H2A, H2B, H3, and H4 was constructed through a collaborator within the lab where this thesis was produced, which was used as the control for all H2A.Z and H2A tailless experiments(*72*). The UV reading during the FPLC run, as well as the subsequently ran 20% polyacrylamide SDS-Page gels, is depicted in **Figure 5**. The subsequent 20% polyacrylamide gels of the pooled octamer fractions are shown in **Figure 6.** Each octamer type was separately reconstituted with purified 208-12 DNA (Figure 1) in a salt dialysis process, and subsequently ran on the AUC absorbance optics to test for the optimal 1:1 nucleosome saturation level of nucleosome binding sites on the DNA through obtaining a S value of approximately 29(*72*). This comparison of each array type used is shown in **Figure 7**(*72*).

Mouse 1 SGRGKQGGKARAKAKTRSSRAGLQFPVGRVHRLLRKGNYSERVGAGAPVYLAAVLEYLTA 60
SGRGKQGGKARAKAK+RSSRAGLQFPVGRVHRLLRKGNY+ERVGAGAPVYLAAVLEYLTA
Human M 1 SGRGKQGGKARAKAKSRSSRAGLQFPVGRVHRLLRKGNYAERVGAGAPVYLAAVLEYLTA 60

Mouse 61 EILELAGNAARDNKKTRIIPRHLQLAIRNDEELNKLLGRVTIAQGGVLPNIQAVLLPKKT 120
EILELAGNAARDNKKTRIIPRHLQLAIRNDEELNKLLGRVTIAQGGVLPNIQAVLLPKKT
Human 61 EILELAGNAARDNKKTRIIPRHLQLAIRNDEELNKLLGRVTIAQGGVLPNIQAVLLPKKT 120

Mouse 121 ESHHKAKGK 129
ESHHKAKGK
Human 121 ESHHKAKGK 129

Figure 4: Mouse H2A vs Tailless Human H2A:

Shown here is the wildtype mouse H2A (top layers) vs the human H2A (bottom layers) amino acid sequences, with the numbers representing the number of amino acids from the N terminus. The conserved amino acids are shown in the middle layer, with the two changes between the two proteins in red. The yellow highlighted amino acids represent those deleted in the human H2A double tailless construct used in this thesis. The tailless human construct also has a methionine (M) at the N terminus, which the recombinant wildtype mouse H2A lacks. The double tailless mutant loses four positive charges from the H2A N terminal tail, and a net of 3 positive charges from the c terminal tail (4 lysine amino acids minus a negatively charged glutamate). Sequences were compared using NIH's BLAST website.

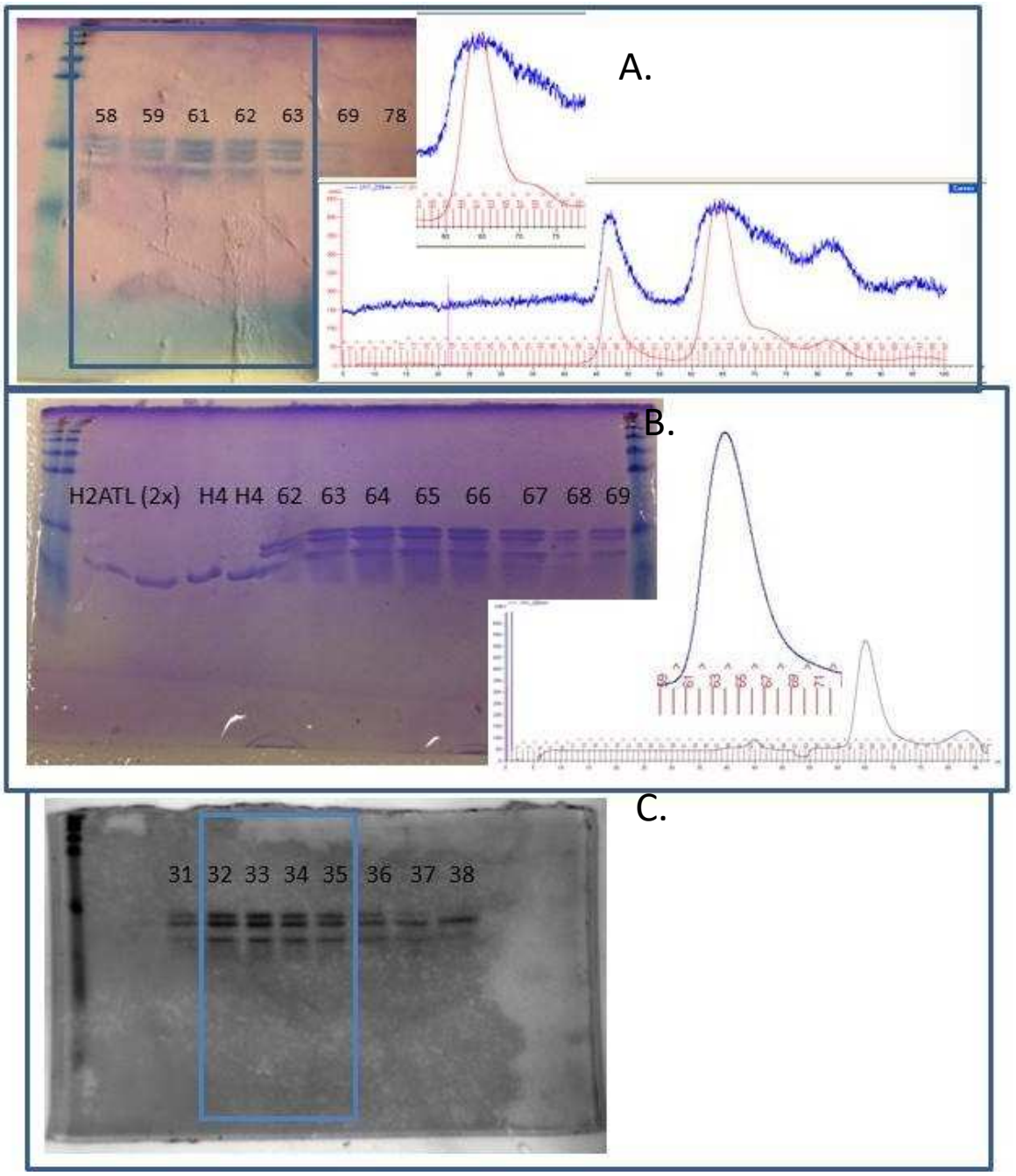

Figure 5: Purification of H2A.Z, H2A Tailless, and Wildtype Octamers:
Depicted are the 20% polyacrylamide SDS-Page gels of histone octamer fractions from the FPLC purification runs. The labeled fractions that were pooled and concentrated for use are bracketed in blue. The UV absorbance spectrum for the FPLC run is also shown for H2A.Z and H2A tailless octamers (280nm=red in A, 280nm=blue in B), with an additional zoomed in image on the octamer peak. A. H2A.Z octamer. B. H2A tailless (TL) octamer. C. Wildtype octamers(73), adapted from McDonald, C. J. (2016) Unpublished Work: Wildtype Octamer and Wildtype Nucleosomal Array Construction, Colorado State University, Fort Collins, CO.

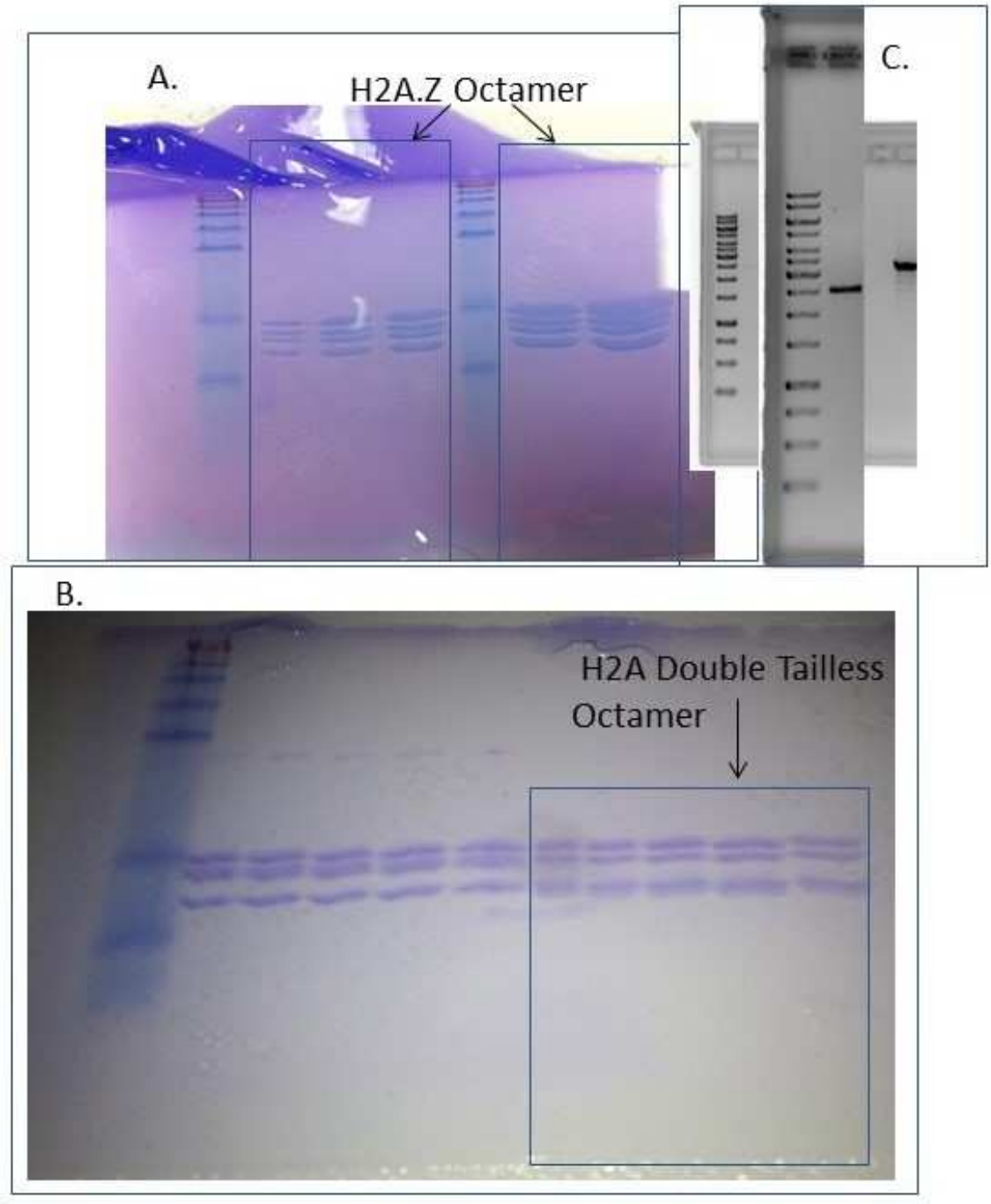

Figure 6: Octamers and DNA Used for Nucleosomal Arrays:
After the fractions from the FPLC were ran on a gel, the fractions of highest purity were pooled and concentrated and then ran on the 20% polyacrylamide SDS-Page gels depicted here. This was the last check for purity and histone ratios before they were assembled with DNA into arrays. The DNA used is also shown. **A.** H2A.Z octamers. **B.** H2A tailless octamer in bracketed lanes. **C.** Background: 208-12 DNA used for H2A tailless arrays. Foreground: 208-12 DNA used for wildtype and H2A.Z arrays.

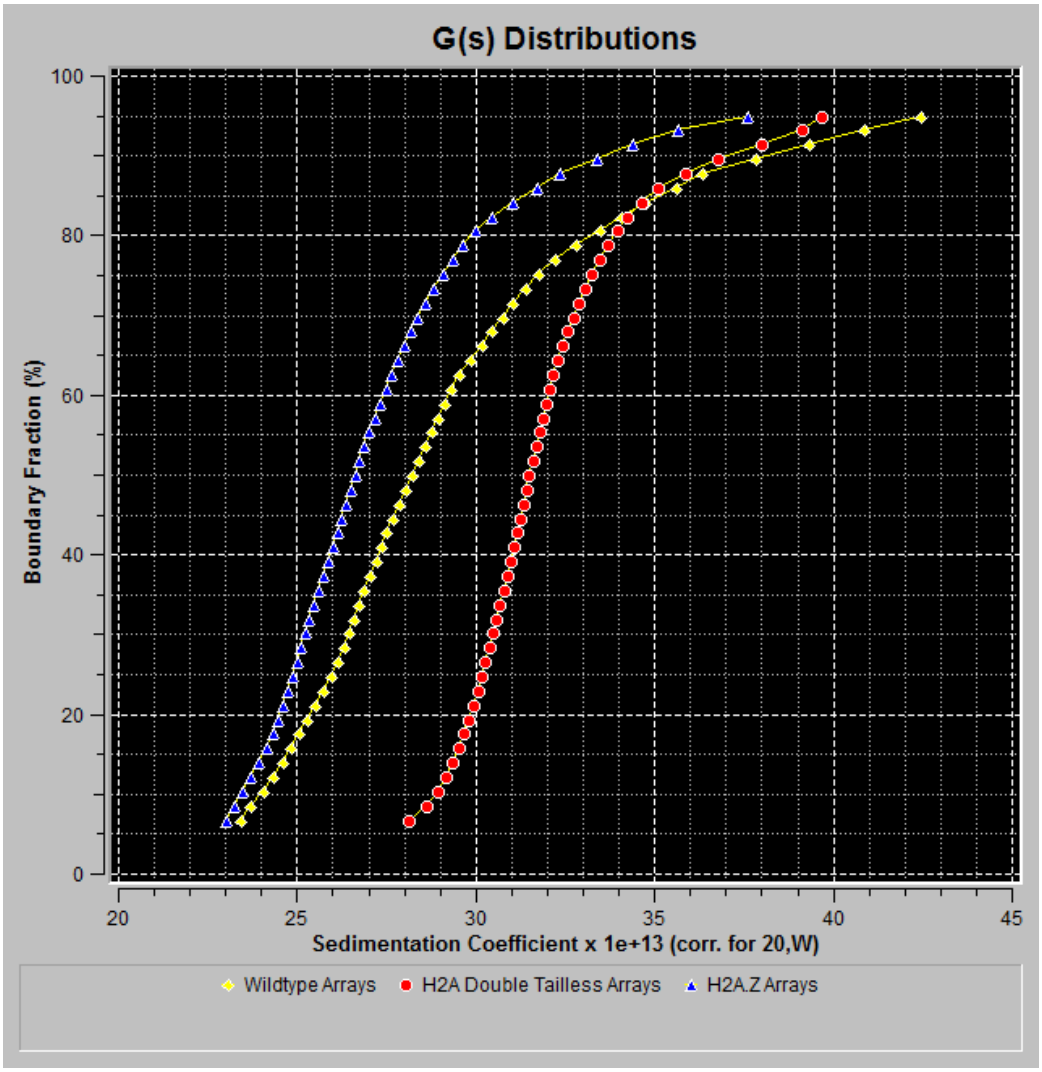

Figure 7: Sedimentation Value Distribution of Nucleosomal Arrays:
The diffusion-corrected S value distributions obtained from absorbance optics sedimentation velocity analytical ultracentrifugation for the wildtype arrays (yellow)(*73*), H2A double tailless arrays (red), and H2A.Z arrays (blue) is shown. Data analysis and graph used UltraScan-3 software. Increased ratios of nucleosome per nucleosome binding site on the DNA increase the S value, which is indicative of the histone octamer: DNA nucleosome binding site molar ratio. Wildtype array part adopted from McDonald, C. J. (2016) Unpublished Work: Wildtype Octamer and Wildtype Nucleosomal Array Construction, Colorado State University, Fort Collins, CO.

3.2: Differential Centrifugation Assay

The differential centrifugation curves for the H2A.Z arrays, H2A tailless arrays, and both wildtype arrays are shown in **Figure 8**, with approximately half of the wildtype data from a laboratory collaborator(*72*). The wildtype arrays oligomerized around 2.5mM $MgCl_2$ with a 50% oligomerization Mg

concentration slightly less than 1.5mM Mg(*72*). In comparison, the H2A tailless arrays were 50% oligomerized between 2.25 and 2.75 mM Mg, and fully oligomerized between 3-4.5 mM Mg.

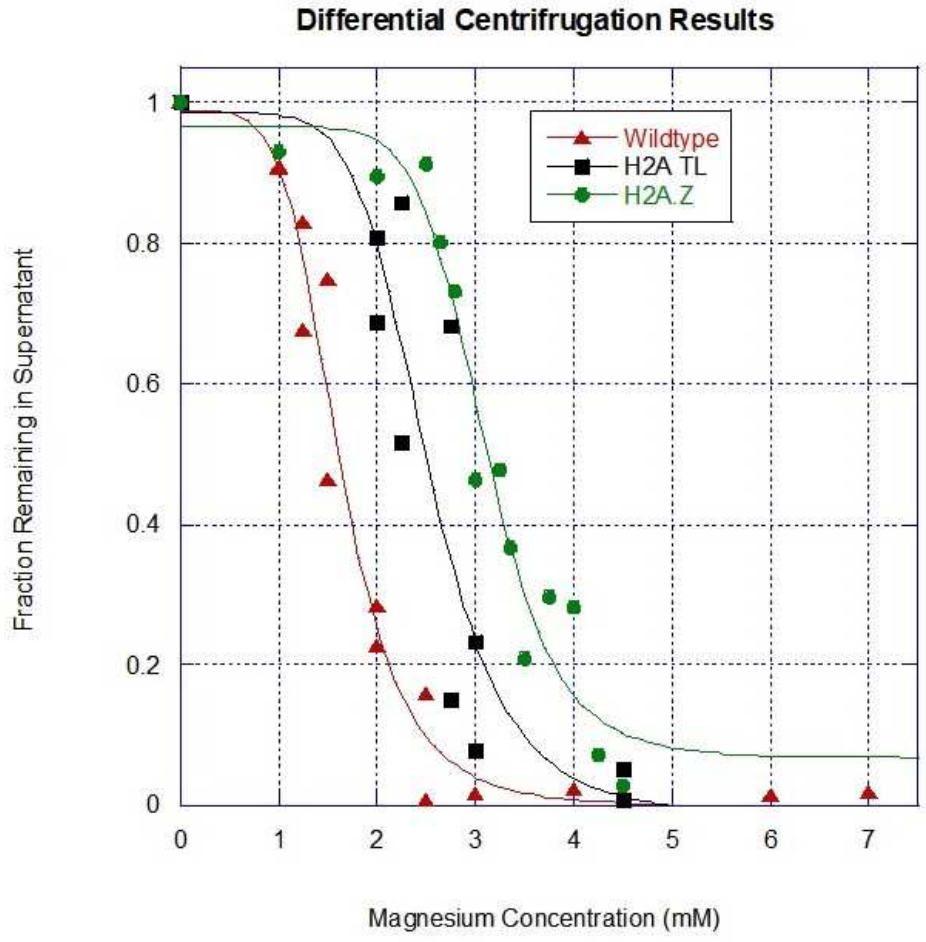

Figure 8: Differential Centrifugation Results:
Shown here are the differential centrifugation results of wildtype (WT, red), H2A tailless (TL, blue), and H2A.Z (green) arrays. Kaleidagraph software was used. The absorbance values measured after the centrifuge spin were divided by the average 0mM Mg absorbance of that array type. The 0mM absorbance is therefore set to 1. Approximately half of the wildtype data set, approximately one replicate, was from a laboratory collaborator(*72*), McDonald, C. J. (2016) Unpublished Work: Wildtype Octamer and Wildtype Nucleosomal Array Construction, Colorado State University, Fort Collins, CO.

The H2A.Z arrays also required more Mg to oligomerize compared to the wildtype arrays(*72*), reaching 50% oligomerization between 2.8 and 3.25 mM Mg and fully oligomerizing around 4.5 mM Mg.

3.3: Micrococcal Nuclease Results

Micrococcal nuclease digested wildtype arrays faster in 3.27mM $MgCl_2$ than in 0 mM $MgCl_2$ (**Figure 9**). The differential centrifugation assay suggested that these arrays should be oligomerized at 3.27mM $MgCl_2$, hinting at a likely more condensed and more challenging to digest formation, such that the arrays in 3.27mM $MgCl_2$ should have a slower digestion rate than the arrays in 0mM $MgCl_2$. Thus, as a control, naked non-nucleosome bound 208-12 DNA was subjected to the same protocol at varying magnesium concentrations, depicted in **Figure 10**. Micrococcal nuclease requires calcium as a cofactor to function, and it was possible that magnesium could substitute for calcium to at least some extent, possibly explaining the faster array digestion rate at 3.27mM than at 0mM $MgCl_2$. Naked DNA does not undergo divalent cation dependent oligomerization as nucleosomal arrays do(*30*), so in theory its digestion rate by micrococcal nuclease would not be affected by varying the magnesium concentrations. This is supported by the naked DNA control digestion, as the rate of digestion increased from 0mM to 0.47mM $MgCl_2$ but was relatively constant at magnesium concentrations from 0.47 to 4.68 mM $MgCl_2$, suggesting that $MgCl_2$ has a slight impact on micrococcal nuclease digestion rate but that working with higher magnesium concentrations does not affect the enzyme's activity. A more complete digestion pattern of naked 208-12 DNA at 7mM $MgCl_2$ can be located in **Figure 11**.

Wildtype and H2A.Z arrays had relatively similar digestion rates at 7mM $MgCl_2$ (**Figures 13**-**14**), as well as at 3.27mM $MgCl_2$ (**Figure 12**). This comparison was analyzed in **Figure 15.** H2A tailless arrays had slightly slower digestion rates at 7mM $MgCl_2$ (**Figures 16-17**), as analyzed by the disappearance of the full-length array DNA sequence in **Figure 18.**

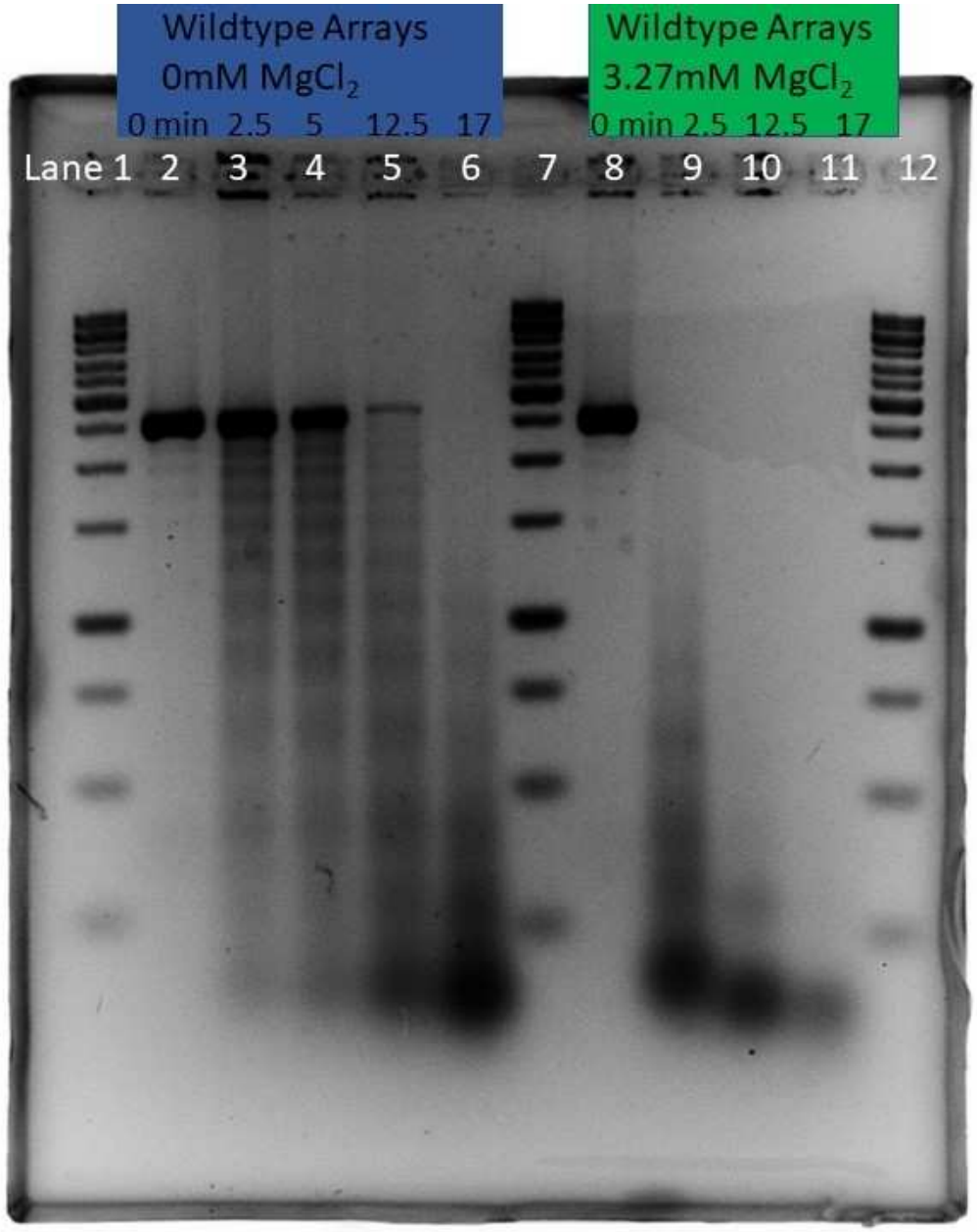

Figure 9: Wildtype Arrays 0mM Mg vs 3.27mM Mg Micrococcal Nuclease Digest:
Wildtype Arrays were incubated in 0mM $MgCl_2$ (lanes 2-6) or in 3.27mM $MgCl_2$ (lanes 8-11) for 15 minutes on ice. They were then digested at 37 C° with micrococcal nuclease for 0, 2.5, 5, 12.5, or 17 minutes. The samples were then phenol chloroformed, alcohol precipitated, and re-suspended in TE before being ran on a 2% agarose gel. Lanes 1 and 12 are ThermoFisher's 1kb ladder, where the 8^{th} band from the top represents 2,500 base pairs.

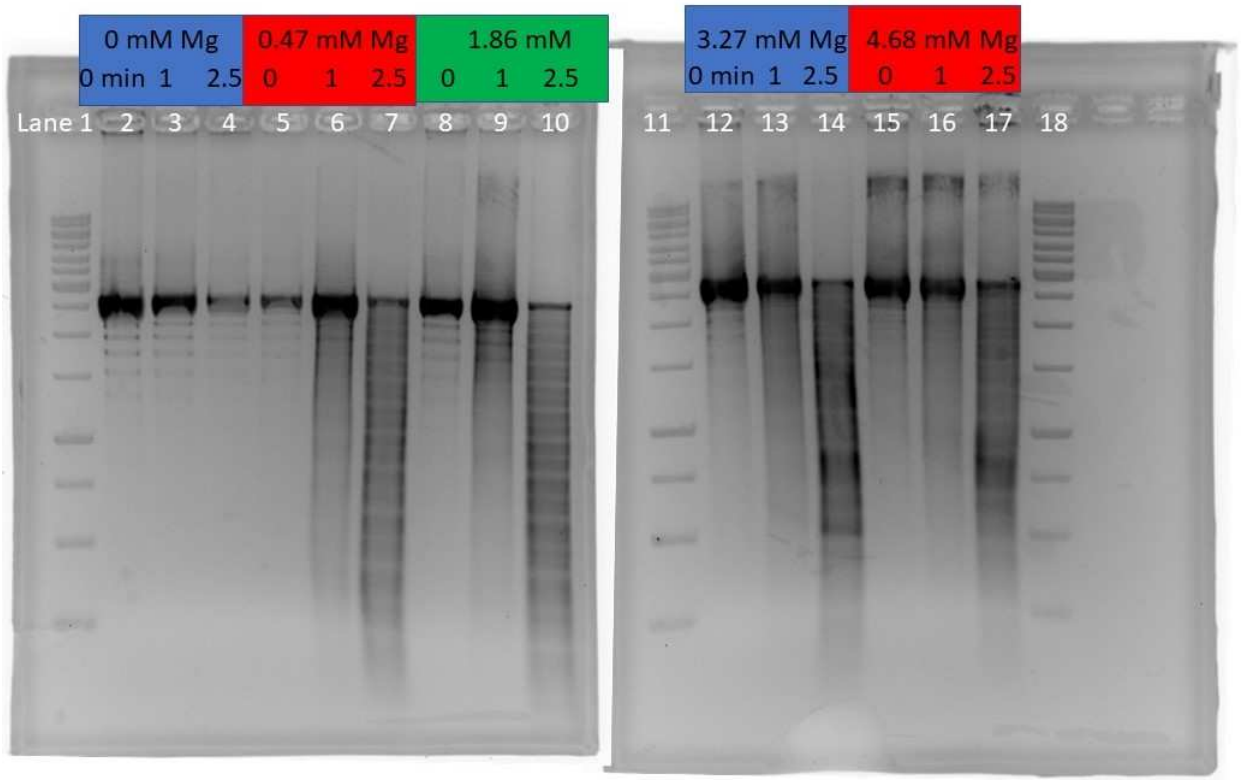

Figure 10: Micrococcal Nuclease of Naked DNA from 0-4.68mM Mg:
Naked 208-12 DNA was digested for 0, 1, and 2.5 minutes (0, 1, and 2.5) at 37 C° at 0, .47, 1.86, 3.27, and 4.68mM magnesium chloride concentrations. This acted as a control to test what effect Mg concentrations had on micrococcal nuclease enzymatic activity, as it and the enzyme's preferred catalyst, calcium, are both divalent cations. There was an increased digestion of the 208-12 DNA in 0.47mM $MgCl_2$ compared to the 0mM concentration digests. However, there was no increase in digestion rate of the DNA with increased magnesium concentrations beyond 0.47 mM magnesium, likely showing that the increased digestion rates in magnesium concentrations in nucleosomal arrays in magnesium concentrations above around 0.47mM magnesium are not due to increased magnesium concentrations. It is more likely that this is due to different accessibility of the linker DNA though the oligomerization of nucleosomal arrays at the higher magnesium chloride concentrations.

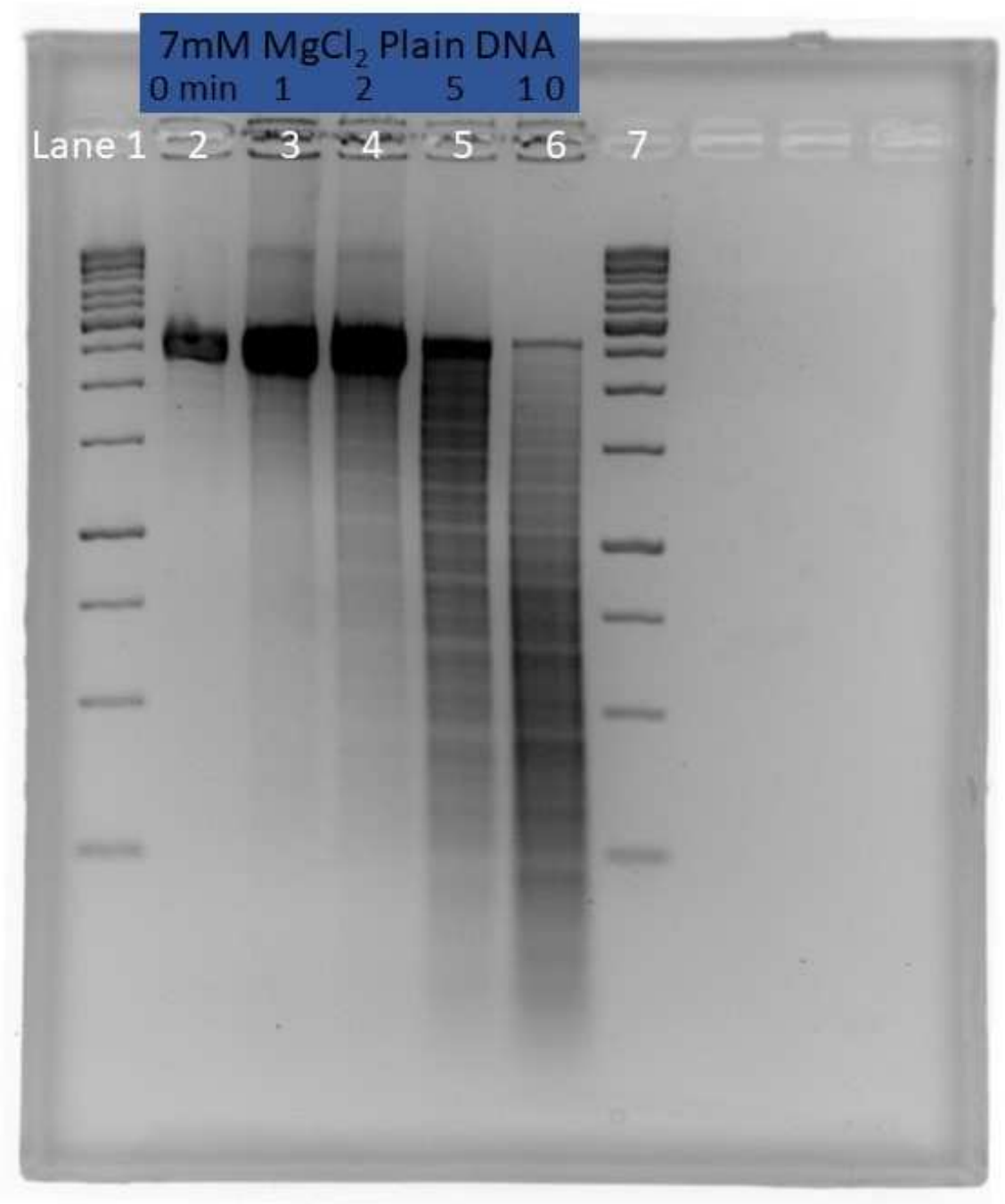

Figure 11: Micrococcal Nuclease of Naked DNA at 7mM Mg:

Naked DNA (lanes 2-6) was incubated in 7mM $MgCl_2$ for 15 minutes on ice before being digested with micrococcal nuclease for 0, 1, 2, 5, and 10 minutes at 37 C°. The samples were then phenol chloroformed, alcohol precipitated, and re-suspended in TE before being ran on a 2% agarose gel. Lanes 1 and 7 is ThermoFisher's 1kb ladder, where the 8^{th} band represents 2,500 base pairs.

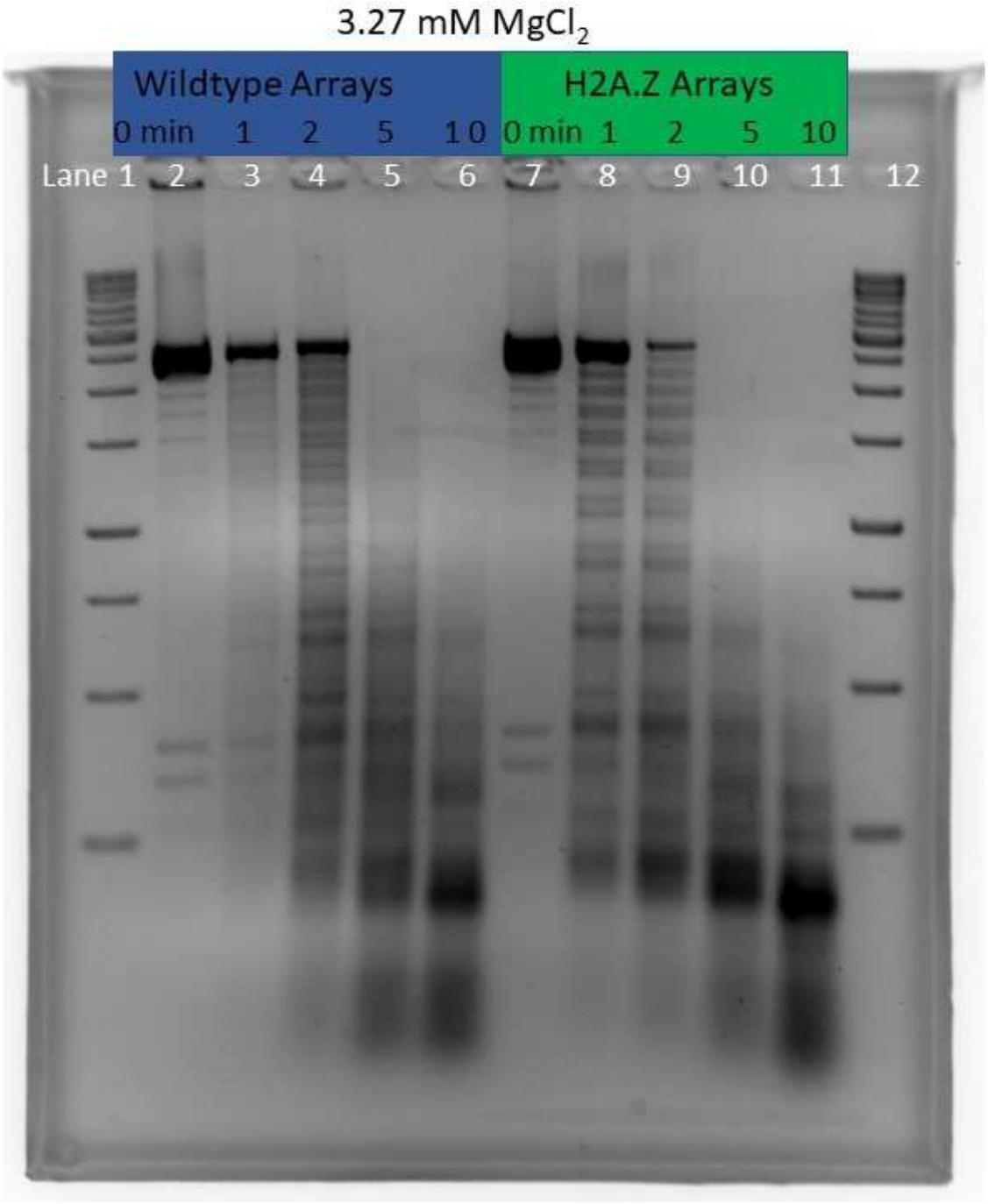

Figure 12: Wildtype vs H2A.Z Arrays Micrococcal Nuclease Digest at 3.27mM Mg:
Wildtype arrays (lanes 2-6) and H2A.Z arrays (lanes 7-11) were incubated in 3.27mM $MgCl_2$ for 15 minutes on ice before being digested at 37C with micrococcal nuclease for 8minutes (naked DNA) or for 0, 1, 2, 5, and 10 minutes at 37 C°. The samples were then phenol chloroformed, alcohol precipitated, and re-suspended in TE before being ran on a 2% agarose gel. Lanes 1 and 10 are ThermoFisher's 1kb ladder, where the 8th band represents 2,500 base pairs.

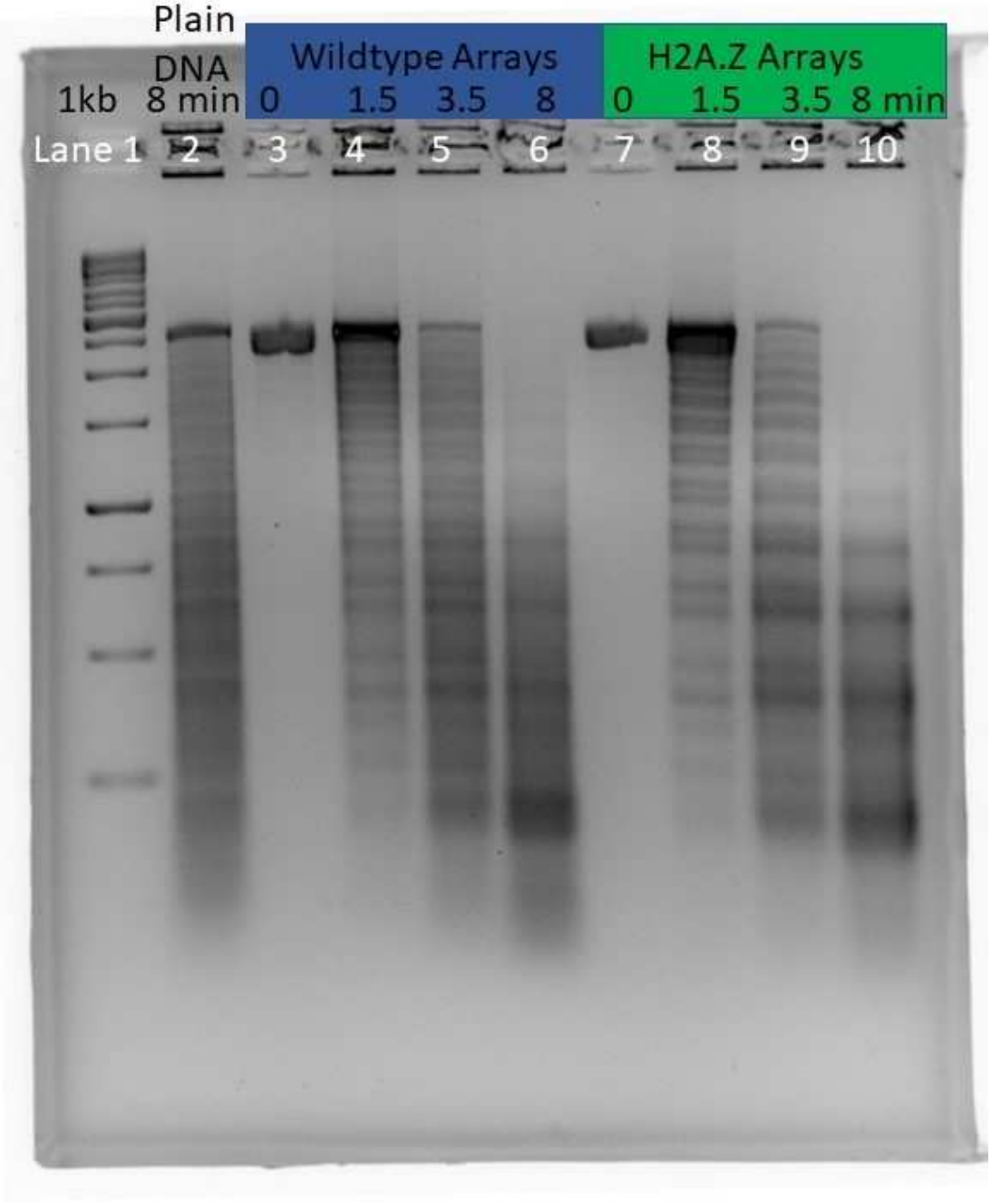

Figure 13: Wildtype vs H2A.Z Oligomerized Arrays Micrococcal Nuclease Digest at 7mM Mg:
This is one of three representative gels of the wildtype vs H2A.Z oligomerized arrays digestion, with the other representations in **Figure 14.** Naked DNA (lane 2), wildtype arrays (lanes 3-6) and H2A.Z arrays (lanes 7-10) were incubated in 7mM magnesium for 15 minutes on ice before being digested at 37C with micrococcal nuclease for 8minutes (naked DNA) or for 0, 1, 2, 5, and 10 minutes at 37 C° (arrays). The naked DNA was digested with one-fifth the number of units of enzyme per microgram of DNA compared to the arrays. The samples were then phenol chloroformed, alcohol precipitated, and re-suspended in TE before being ran on a 2% agarose gel. Lane 1 is ThermoFisher's 1kb ladder, where the 8th band represents 2,500 base pairs.

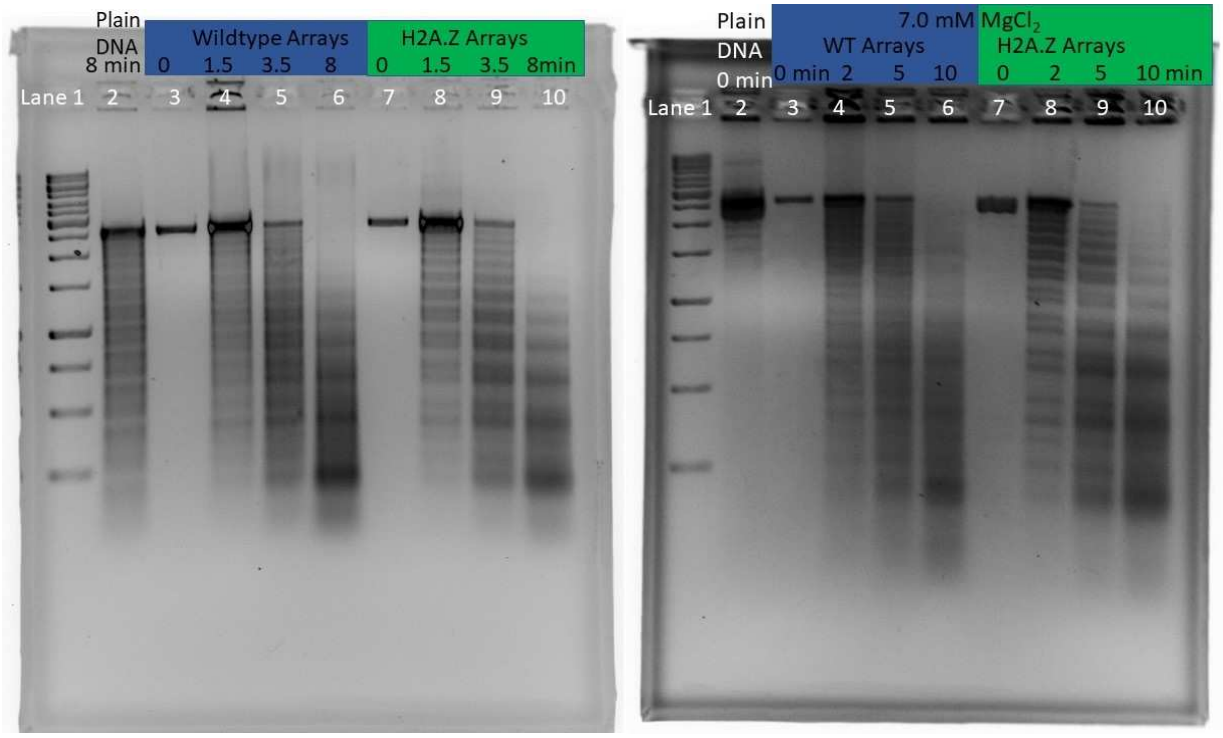

Figure 14: Wildtype vs H2A.Z Oligomerized Arrays Micrococcal Nuclease Digest at 7mM Mg:
Two representative gels of wildtype vs H2A.Z oligomerized array micrococcal nuclease digestions are shown here, in addition to the one in **Figure 13.** Naked DNA (lane 2 in each replicate), wildtype arrays (lanes 3-6) and H2A.Z arrays (lanes 7-10) were incubated in 7mM magnesium for 15 minutes on ice before being digested at 37C with micrococcal nuclease for 8 or 0 minutes (naked DNA) or for 0, 1, 2, 5, and 10 minutes at 37 C° (arrays). One-fifth of the units of enzyme per microgram of DNA was used for the naked DNA compared to the arrays. The samples were then phenol chloroformed, alcohol precipitated, and re-suspended in TE before being ran on a 2% agarose gel. Lane 1 is ThermoFisher's 1kb ladder, where the 8th band represents 2,500 base pairs.

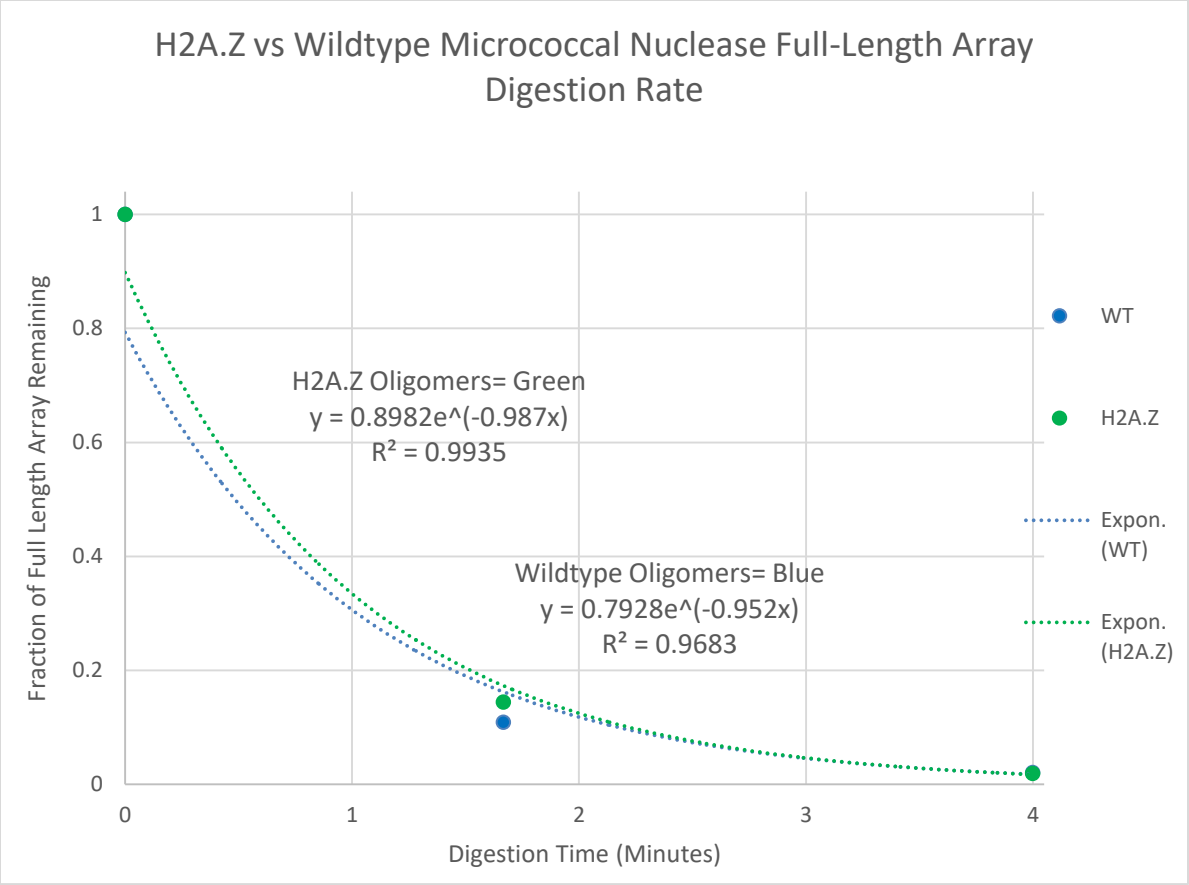

Figure 15: H2A.Z Oligomers Micrococcal Nuclease Gel Analysis:
For each micrococcal nuclease representative gel, the intensity of the top band of each array type at each time point where the band was present was divided by the top band's intensity of the 0-minute digestion time point for that representative gel, which was then averaged across the three representative gels. One-tenth of the amount of DNA of the 0 minute digest was loaded onto the gels compared to the amount of loaded DNA for the other time points, and thus each 0 minute time point's band intensity was multiplied by ten to correct for this. The full-length DNA band's intensity was not measurable at the last digestion time point (at 8 or 10 minutes). The top band represents an undigested 208-12 DNA sequence, corresponding to a nucleosomal array pre-phenol wash. The intensities were then graphed and fitted to an exponential function. H2A.Z oligomers had a similar digestion rate compared to wildtype oligomers as measured by the disappearance of the full 208-12 DNA sequence.

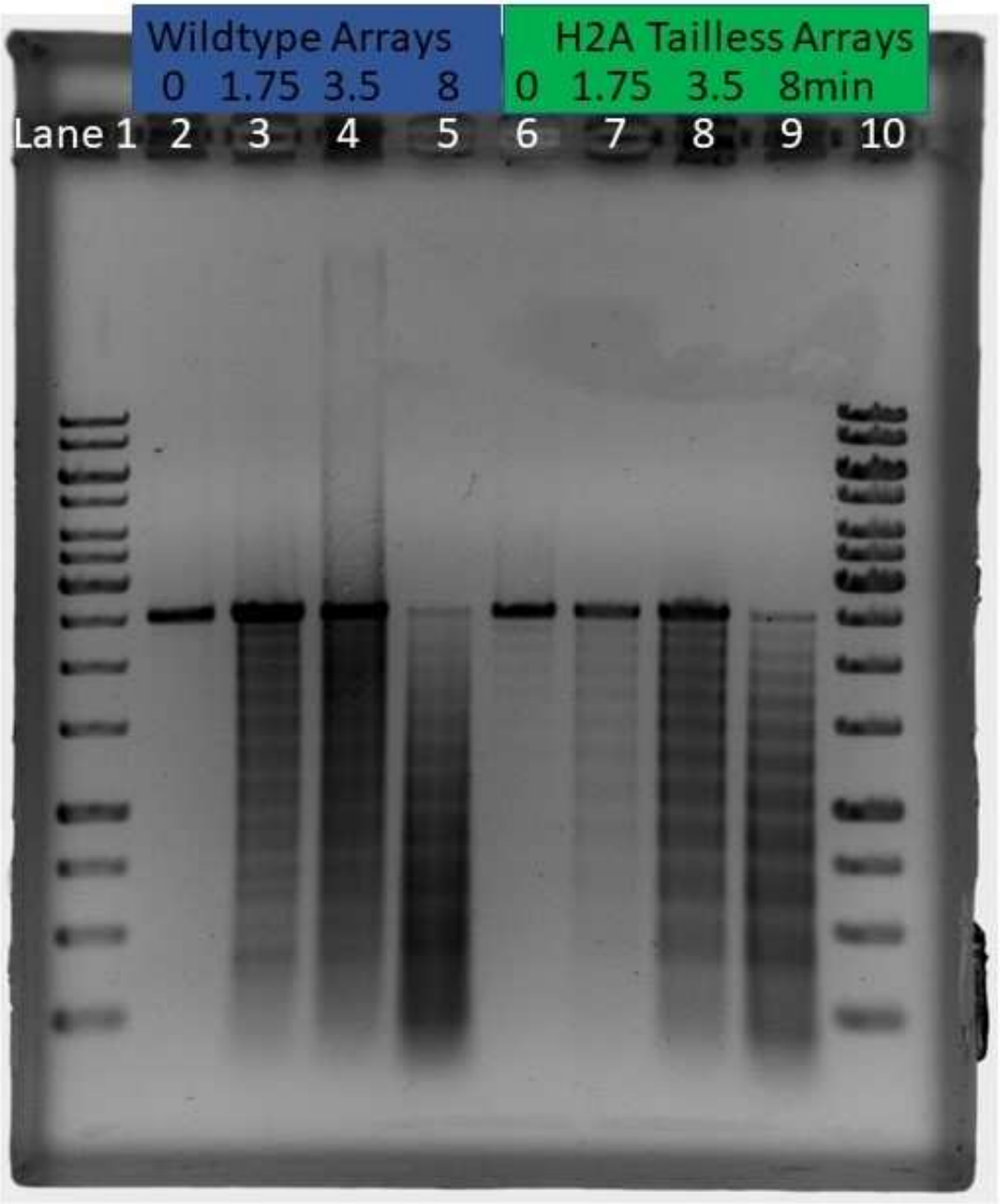

Figure 16: Wildtype vs H2A Tailless Oligomerized Arrays Micrococcal Nuclease Digest at 7mM Mg:
One representative gel of wildtype versus H2A.Z oligomerized arrays micrococcal nuclease digestions is shown here, with the other two representations depicted in **Figure 17.** Micrococcal nuclease digests at 7mM $MgCl_2$ of wildtype and H2A double tailless arrays. Lane 1: 1kb ThermoFisher ladder. Lane 2: naked DNA control. Lanes 3-6: 0, 1.5, 3.5, or 8 minute micrococcal nuclease digest DNA products. Lanes 7-10: 0, 1.5, 3.5, and 8 minute H2A double tailless micrococcal nuclease digest products.

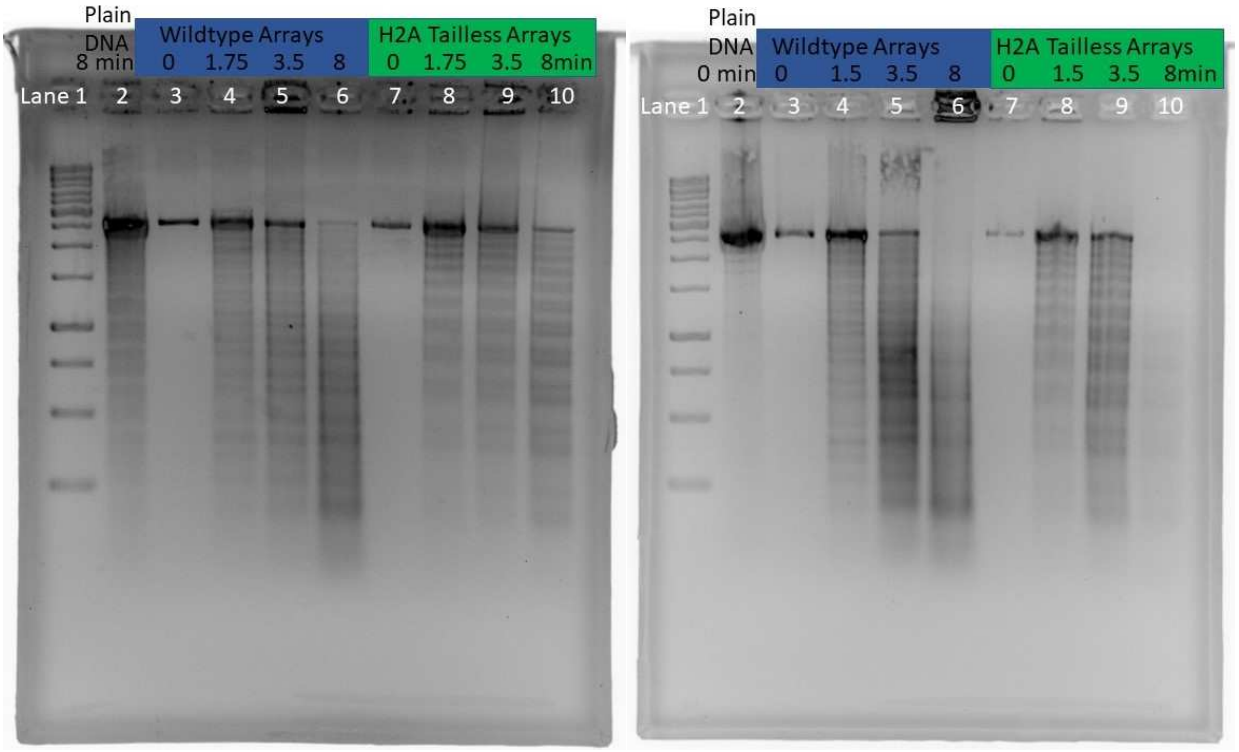

Figure 17: Wildtype vs H2A Tailless Oligomerized Arrays Micrococcal Nuclease Digest at 7mM Mg: Two representative gels of wildtype vs H2A double tailless oligomerized array micrococcal nuclease digestions are shown here, in addition to the one in **Figure 16.** Naked DNA (lane 2 of each gel), wildtype arrays (lanes 3-6 of each gel) and H2A.Z arrays (lanes 7-10 of each gel) were incubated in 7mM $MgCl_2$ for 15 minutes on ice before being digested at 37C with micrococcal nuclease for 8 or 0 minutes (naked DNA) or for 0, 1, 2, 5, and 10 minutes at 37 C° (oligomerized arrays). The naked DNA was digested with one-fifth the number of units of enzyme per microgram of DNA compared to the amount used for the arrays. The samples were then phenol chloroformed, alcohol precipitated, and re-suspended in TE before being ran on a 2% agarose gel. Lane 1 is ThermoFisher's 1kb ladder, where the 8th band represents 2,500 base pairs.

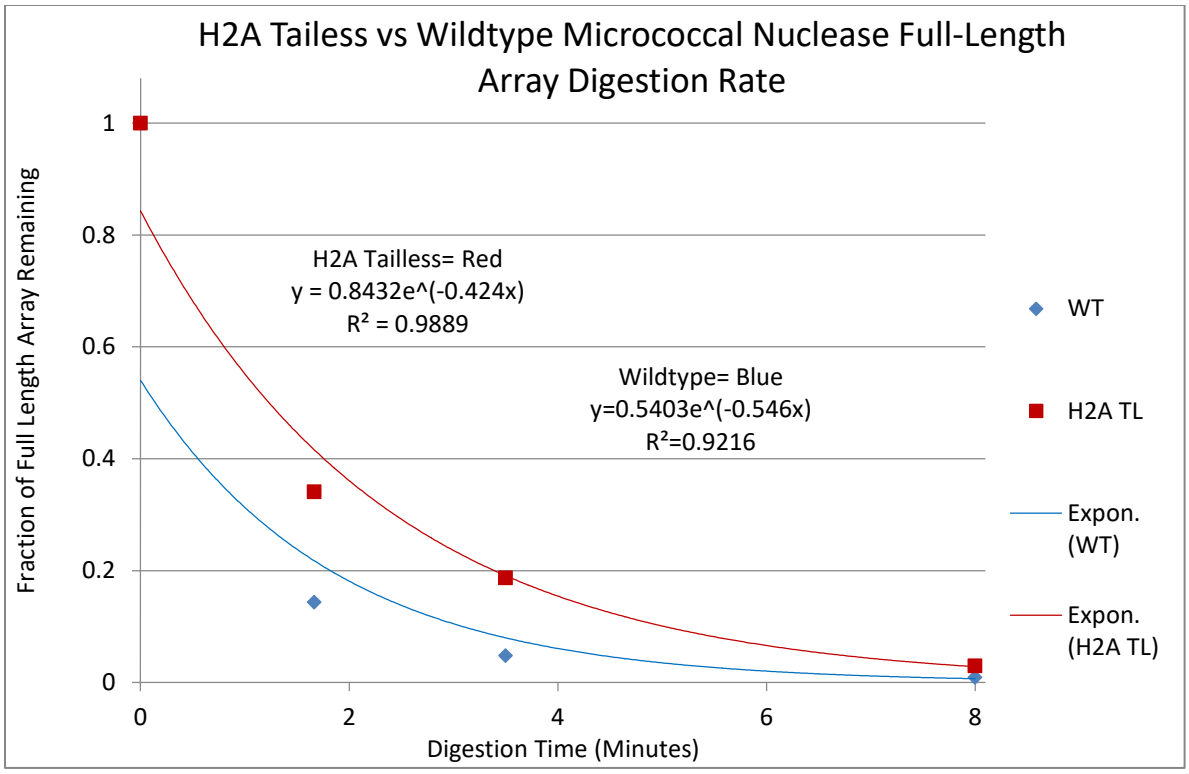

Figure 18: H2A Tailless Oligomers Micrococcal Nuclease Gel Analysis:
For each micrococcal nuclease representative gel, the intensity of the top band of each array type at each time point where the band was present was divided by the top band's intensity of the 0-minute digestion time point for that representative gel, which was then averaged across the three representative gels. One-tenth of the amount of DNA of the 0 minute digest was loaded onto the gels compared to the amount of loaded DNA for the other time points, and thus each 0 minute time point's band intensity was multiplied by ten to correct for this. The top band represents an undigested 208-12 DNA sequence, corresponding to a nucleosomal array pre-phenol wash. The intensities were then graphed and fitted to an exponential function. The last oligomer digestion time point's top band intensity was not measurable on **Figure 17**'s right gel representative gel due to low overall intensity across all bands at this digestion time point, and thus only two representative gel bands were used for the last digestion time point. The full-length 208-12 DNA band disappeared slower for the H2A tailless oligomers compared to wildtype, corresponding to a likely slightly slower digestion rate.

3.4: Fluorescence Recovery After Photobleaching (FRAP) and Imaging

Fluorescence imaging was performed on both the H2A tailless and the H2A.Z arrays that were both constructed by the author, as well as on the wildtype arrays, through collaborators within in the laboratory where the thesis was done(*72, 74*). FRAP was also performed on both H2A.Z and wildtype arrays also with a laboratory collaborator(*72, 74*). The microscope used required FRAP-associated maintenance on two separate occasions when the author prepared H2A tailless, H2A.Z, and wildtype

array slides, and thus the previous H2A.Z and wildtype array samples are used in this thesis with no H2A tailless array FRAP data. Representative images of wildtype, H2A double tailless, and H2A.Z arrays are shown in **Figure 19**(*72, 74*). Although no quantitative analysis was executed on the morphology, all three array types produced seemingly globular oligomers(*72, 74*). The wildtype and H2A tailless oligomers were globular and relatively spherical in shape(*72, 74*).

The FRAP results are found in **Figure 20**(*72, 74*). Both the wildtype and H2A.Z arrays were composed of three different mobility fractions(*72, 74*). The first of these was an immobile fraction, the fraction of the oligomer whose photobleached fluorescence did not recover(*72, 74*). This is likely due to an inability of this array portion to diffuse outwards after the photobleaching time point(*72, 74*). In the H2A.Z arrays, this population composed approximately 20% of the total oligomers tested, compared to an estimated 50% for the wildtype arrays(*72, 74*). The other two populations fit within the mobile fraction, the remaining portion of the oligomer whose fluorescence did recover likely due to the fluorescently tagged octamer bound DNA moving both into and out of the bleached region(*72, 74*). In the H2A.Z samples, a fast recovering population composed 29.7% of the mobile fraction (~23% of the total population), which had a half-life recovery time of 77.02 milliseconds(*72, 74*). This contrasted to the wildtype arrays, whose smaller fast-recovering population accounted for 13.5% of the mobile fraction (~6% of the total population), whose fluorescence recovered at a slower rate with a half-life of 157.5 milliseconds(*72, 74*). In the H2A.Z oligomers, the remaining 70.28% of the mobile fraction (56.22% of the total population) recovered to half of its relative intensity within 13,563.4 milliseconds(*72, 74*). The corresponding wildtype slower-recovering portion reached half its maximum fluorescence at a comparatively faster time of 1,386.3 milliseconds, and this population represented 86.48% of the mobile fraction (83.24% of the total population) (*72, 74*). The recovery data for H4 tailless and acidic patch neutralized array types are depicted as well (*72, 74*).

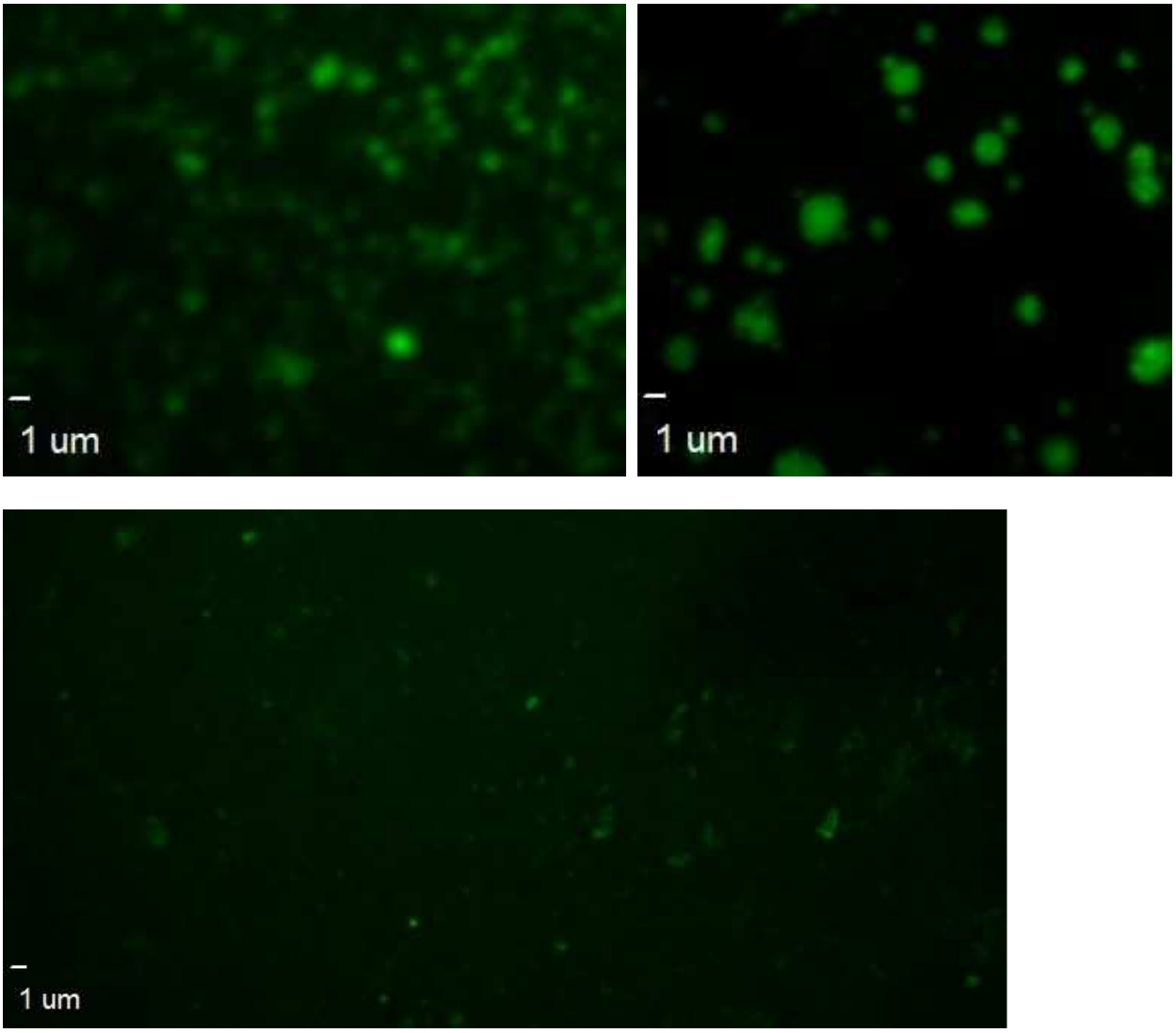

Figure 19: Fluorescence Images of Oligomerized Arrays:
Depicted are oligomers of wildtype arrays at 6mM $MgCl_2$ (top left), oligomers of H2A tailless arrays (top right) at 7mM $MgCl_2$, and H2A.Z oligomers of H2A.Z arrays at 6mM $MgCl_2$, (bottom), with the images from laboratory collaborators (*72, 74*). The oligomers were globular in shape(72, 74). Adopted from Connolly M. and McDonald, C. J. (2017) Unpublished Work: FRAP Data and Images, Colorado State University, Fort Collins, CO.

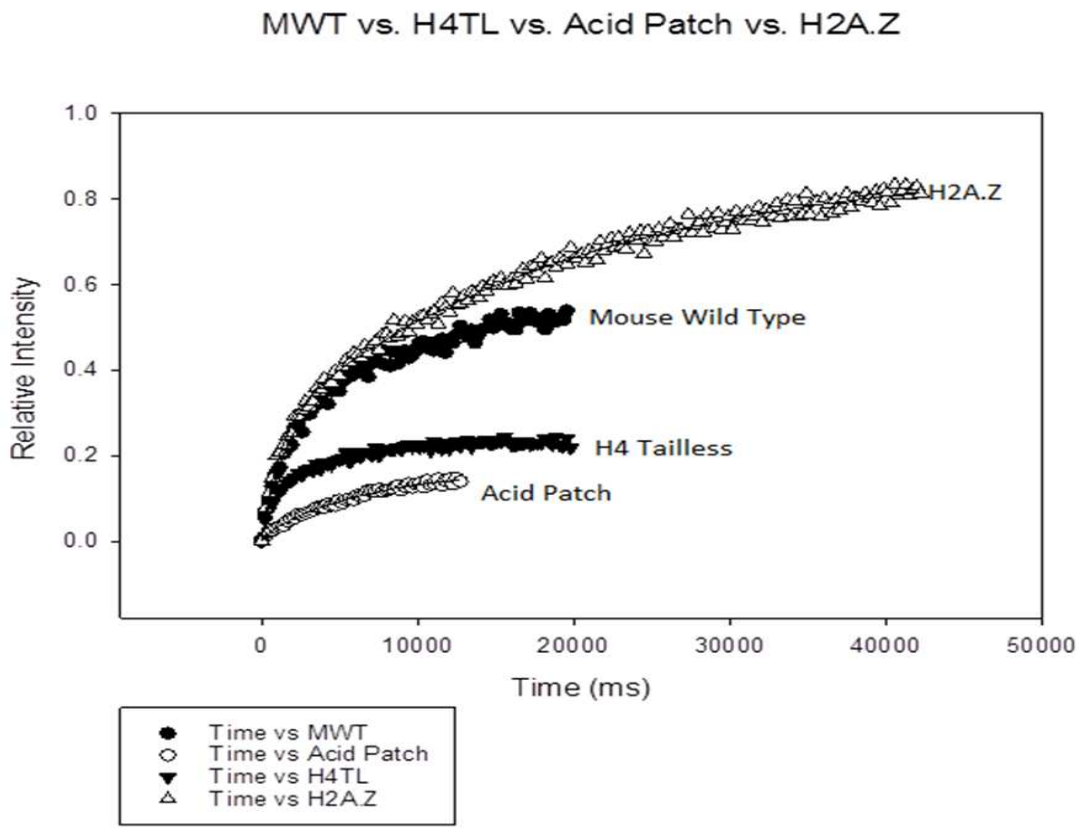

Array Type	Percent of Population 1	Rate Constant (1/ms)	Half Life (ms)	Percent of Population 2	Rate Constant (1/ms)	Half Life (ms)
WT	0.1352	0.0044	157.5	0.8648	0.0005	1386.3
H2A.Z	0.29716	0.0009	77.02	0.70284	0.00005148	13463.4

Figure 20: Fluorescence Recovery After Photobleaching Results:
Depicted at the top is the time after photobleaching versus the relative intensity of the photobleached oligomer for wildtype and H2A.Z arrays(*72, 74*). The chart at the bottom illustrates the distribution of recovering populations and their respective rate constants and half-lives, also from laboratory collaborators (*72, 74*). Acidic patch mutant and H4 tailless mutant array data is also shown(*72, 74*). This work, through laboratory collaborators, was adopted from Connolly M. and McDonald, C. J. (2017) Unpublished Work: FRAP Data and Images, Colorado State University, Fort Collins, CO.
Also adopted from McDonald, C. J. (2017) Role of the H4 N-terminal tail and nucleosome acidic patch in chromatin oligomer dynamics, In *Deparment of Biochemistry and Molecular Biology*, Colorado State University, Fort Collins, CO.

CHAPTER 4: DISCUSSION

4.1: Micrococcal Nuclease Method Results

In addition to magnesium acting as a weaker cofactor for the micrococcal nuclease enzyme, it is also possible that the calcium used in the 3.27mM MgC_2 digestion not only acted as a micrococcal nuclease cofactor but also as an oligomerization agent similar to magnesium. This small amount of calcium chloride used for the micrococcal nuclease might be more likely to bind to -non-oligomerized than to already oligomerized arrays, thus slightly compacting the 0mM $MgCl_2$ arrays and also providing less calcium to propel the enzyme's digest. Adding magnesium to the micrococcal nuclease enzyme just before adding this mixture to the arrays might be a fashion to test this.

4.2: H2A.Z Arrays Discussion

It is reported here that the H2A.Z magnesium induced oligomerization curve was shifted to the right compared to the wildtype control arrays, with part of the wildtype data from laboratory collaborators(*72*) (**Figure 8**). This translates to an increased magnesium concentration necessary to produce the oligomerized state as measured by the 260nm absorbance reading after centrifugation(*72*). It was previously discovered that H2A.Z differential centrifugation curve was shifted to the right compared to canonical arrays for the 0-1mM zinc range (*75*). As noted earlier, three major changes exist between HA.Z and H2A: an extended acidic patch, an altered H2A.Z-H2A.Z L1 loop interaction, and a weakened H2A.Z c-terminal docking domain interaction with H3 and H4 (*46*). While the L1 loop and docking domains have limited known relationship to higher-order structure partially due to minimal research, the acidic patch is known to bind to the H4 tail in array folding (*75*). More importantly, neutralizing H2A's six contributions to the acidic patch shifted the magnesium induced oligomerization curve to the left (*76, 77*), although more recent research with the same model system as used in this lab with a mutated acidic patch found an identical oligomerization curve to the wildtype control(*72*). As

H2A.Z essentially neutralizes a lysine charge found in H2A and adds a negative charge, a net negative charge of four per nucleosome must now be neutralized for the overall negatively charged nucleosomal array to associate(*46*). Thus it is possible that the H2A.Z arrays require more magnesium for the oligomerization process as reported by the magnesium curve in this thesis as a result of the H2A.Z extended negatively charged acidic patch(*72*).

There was minimal noticeable difference between the digestion rates of the H2A.Z and wildtype arrays (**Figures 13-14**), as analyzed in **Figure 15**. As micrococcal nuclease cuts linker DNA before the more shielded nucleosomal DNA (*56*), and since this DNA must be accessible to the enzyme to be diced, it is likely that the array types have similar linker DNA accessibilities, with the H2A.Z arrays digested at a possibly slightly faster rate. Along this line, it is likely that all of the linker DNA is accessible. This suggests that neither H2A nor H2A.Z alone produces a linker DNA inaccessible array state. This is reinforced by the finding of a fluorescent protein's accessibility to diffuse in chromatin and likely reach a target site composed of 10nm fibers (*69*).

The acidic patch is known to interact with the H4 tail in folding(*76*), likely forming a more compact structure(*78*) than the globular mesh of interdigitated 10nm fibers that this current model system uses (*4*). While increased acidic patch-H4 tail interaction occurs with increasing magnesium concentrations (*79*), and H2A.Z increases folding compared to wildtype arrays (*80*), array folding and array oligomerization are competitive processes as previously reviewed (*81*). Thus, it could be hypothesized that less inter-fiber contacts should occur in H2A.Z arrays than in wildtype arrays. Still it was previously suggested that the acidic patch extension on H2A.Z would translate to a more condensed state for H2A.Z arrays compared to arrays of the shorter H2A acidic patch or to acidic patch-less H2A.Bbd variant arrays (*81*). H2A.Z has a greater association with active genes(*82*), but is found in both euchromatin and heterochromatin (*44, 82*). Here, the H2A.Z arrays have similar linker DNA accessibility to canonical H2A arrays. If linker DNA accessibility is indicative of overall array accessibility, and if arrays

are less accessible in a more condensed state, then linker DNA accessibility is also a measure of array compaction. This would suggest that H2A.Z arrays are on average as compact as H2A wildtype arrays, both in agreement and in contrast with previous findings that found varying associations with both euchromatin and heterochromatin(*82*). Subjecting the oligomerized arrays to interference absorbance optics analytical ultracentrifugation would further experiment with this idea. Post translational modifications, the existence of other histone variants, chromatin remodeling complexes, transcription factors, and other factors would be hypothesized to influence this result.

From the current data, the fluorescence of the H2A.Z oligomers recovered to a greater extent, at ~80%, than that of the wildtype oligomers, at approximately 50%(*72, 74*). Although the wildtype and H2A.Z oligomer FRAP and image data was from laboratory collaborators, the analysis in determining how these results might influence chromatin structure in regards to H2A.Z is a result of the thesis author, and also of the respective cited works in terms of comparing the results to that of previous chromatin studies. The H2A.Z oligomers also had a greater fast-recovering portion of the mobile fraction and overall fraction, 29.7% and 23%, respectively (assuming 80% mobile fraction), than the wildtype arrays at 13.5 and 6%, respectively (assuming 50% mobile fraction) (*72, 74*). This faster recovering portion of the H2A.Z arrays also recovered at a faster rate than that of the wildtype oligomers, with corresponding half-lives of 77.02 milliseconds and 157.5 milliseconds(*72, 74*). This data suggests that the H2A.Z oligomers have an overall increased mobility compared to the wildtype oligomers, and that a majority of this mobile region consists of comparatively rapidly fluctuating arrays(*72, 74*). In contrast, although the slower recovering population composed more of the overall oligomer population in the H2A.Z samples, this fraction moved approximately ten times slower than the corresponding wildtype subset according to the half-lives(*72, 74*).

It was previously reported that the oligomers constructed from the model system used here compared to the sizes of chromatin domains existing in vivo(*3, 4*). Transcription has been hypothesized

to occur around the edges of these structures, as these regions are most readily accessible(*5*). In theory these regions would be least spatially confined to movement and could exchange with other oligomers, or their corresponding domains in vivo, most readily, possibly accounting for the FRAP fast recovering population(*72, 74*). In contrast, more condensed, less accessible, and likely less transcribed heterochromatin is less dynamic and partakes in less movement than other regions(*83*). This description would possibly correlate with the immobile regions(*72, 74*) of the photobleached oligomers. The slower recovering FRAP population(*72, 74*) could correspond to a structural setting whose mobility and compactness is between that of the relatively rapidly fluctuating and the immobile populations. Regardless of their respective mobility, all three of these structural forms are still accessible to a small protein, per the micrococcal nuclease results, without necessitating any post-translational modification, histone remodeling complex, or other assistance. Although FRAP was not performed on H2A tailless arrays, if different populations emerge from those arrays as well, they are hypothesized to be equally accessible based on their micrococcal nuclease results.

In light of the H2A.Z results, the structural hypothesis laid out above would suggest that H2A.Z favors a more mobile(*72, 74*), euchromatin suggestive dynamic over a more rigid and compact but still accessible heterochromatin style organization. The intermediate mobility morphology is less dynamic than what the wildtype H2A offers(*72, 74*). From a protein prospective, the H2A.Z nucleosome's prolonged acidic patch provides additional net negative charges for the positively charged tails to transiently bind to(*46*), and if the tails were able to alter placement of the much larger nucleosome to even a small extent, this could increase the overall mobile fraction. Perhaps this is more likely related to the additional net two negative charges due to H2A.Z's extended acidic patch(*46*), where, according to the differential centrifugation results(*72*), these charges require neutralizing by likely divalent cation and or tail binding to oligomerize. The same $MgCl_2$ concentration of 6mM was used to oligomerize both array types(*72, 74*). Thus, it is likely that the H2A.Z oligomers would also involve more open arrays due

to charge repulsion, possibly leading to the increased mobile fraction and increased mobility of the most fluctuating array population(*72, 74*). However, the overall accessibility remained relatively constant, partially due to the restricted mobility of the still fluctuating but more compact fraction(*72, 74*). A possibility exists that the decreased mobility of the less mobile fraction results from very restricted movement from the percentage of sample that would be immobile in the wildtype oligomers, and not necessary from the demographic that is more rapidly moving in the corresponding wildtype oligomers(*72, 74*).

Although domains whose H2A representative is purely non-post-translationally modified H2A.Z likely does not exist in nature, the association of H2A.Z with both euchromatin and heterochromatin is consistent with results from a human cancer cell line(*82*) as well as in the Drosophila fly(*84*). In human cells, H2A.Z is found around promoters, where it can recruit RNA polymerase II, and in heterochromatin, but not in transcribed genes(*82*). H2A.Z is additionally found around telomeres in yeast(*85*), in mouse and human pericentric heterochromatin(*86*), and in mammalian enhancers(*82*). In this context it is not surprising that an increased most mobile fraction existed in the oligomers per the FRAP results(*72, 74*). Overall, a H2A variant review paper suggested that H2A.Z is more correlated with expressed genes, potentially agreeing with the increased mobile fraction described here(*44, 72, 74*).

An increased mobile fraction, as seen with H2A.Z arrays(*72, 74*), is predicted to contribute to increased structural variability and rearrangement of chromatin. The movement of DNA sequences, including promotors and enhancers, likely influences gene expression, possibly in positive, neutral, and negative fashions, as a DNA region needs to be accessible to transcription factors, promotors, other proteins, and RNA to be transcribed. The same principle would likely also apply to DNA replication in terms of DNA polymerase, and DNA repair with its associated factors. Therefore, the mobility of a specific DNA sequence within a H2A.Z rich oligomer would likely change its downstream protein-associated functional dynamic as a function of time in a structurally based format. Chromatin mobility is

also a property of a euchromatic state, as likely heterochromatin regions displayed less movement in mammalian cells in vivo(*83*), possibly due to less structural constraints. Therefore, this increased mobility(*72, 74*) offers the possibility that H2A.Z promotes a structure more accessible to DNA and histone-associated factors, and accordingly increasing the occurrences of the processes that these factors partake in. However, H2A.Z did not alter the linker DNA accessibility compared to canonical wildtype H2A arrays according to the micrococcal nuclease results, and linker DNA's accessibility to micrococcal nuclease might be an indication with overall accessibility to a generic protein. If FRAP and micrococcal nuclease digestion rates were both indications of accessibility and compactness, these two results regarding the H2A.Z protein might be at odds(*72, 74*). While the micrococcal nuclease assay measures generic linker DNA accessibility, the photobleaching of an entire oligomer in FRAP is more revealing of movement between an oligomer and its environment, although intra-oligomer array dynamics is also required. Therefore, the argument between a more mobile but equally accessible state may not be relevant in the current results due to the different information expressed by the two assays(*72, 74*). Regardless, according to current results, H2A.Z had an overall increased mobile fraction, and also lead to a more mobile and likely more open state in some of its faster recovering FRAP population based on present data(*72, 74*). This faster recovering population(*72, 74*) would be suggested to be more open in a more rapid manner to transcription, DNA replication, DNA repair, chromatin remodeling complexes, epigenetic modifications, and other factors as a result, promoting these processes. Canonical wildtype H2A arrays as well as the remainder of the H2A.Z array populations(*72, 74*) would also be open to these processes, as their entire chromatin structure was digested and accessible to micrococcal nuclease, but possibly in a slower fashion. The slower recovering FRAP population of both H2A.Z and wildtype oligomers(*72, 74*) would be more time-repelling but still submissive to protein binding or DNA or protein modifications. Additionally, the less accessible regions, possibly the less mobile regions according to FRAP(*72, 74*), are thought to be more protected from UV

radiation damage(*87*). Overall, compared to wildtype H2A oligomers, H2A.Z from the results depicted in this thesis is thought to promote a more fluctuating and thus dynamic chromatin state, with possibly increased access to some of its constituents to processes including transcription, chromatin remodeling complexes, DNA repair, and DNA replication(*72, 74*).

The results of the differential centrifugation, micrococcal nuclease, and FRAP assays contrasted with that of the pre-experiment hypotheses(*72, 74*). H2A.Z arrays were predicted to create a more compact structure, translating to less magnesium necessary for oligomerization versus that of the wildtype arrays, a slow micrococcal nuclease digestion rate, and a lower mobile fraction as discovered through FRAP. This was based on the results that the acidic patch was shown to have in array folding, which was thought to translate to some extent to array oligomerization(*76*). In reality, however, H2A.Z arrays required increased magnesium to oligomerize(*72*), produced similarly accessible linker DNA according to the micrococcal nuclease assay, and an increased mobile fraction when compared to wildtype canonical H2A arrays(*72, 74*). This is more in line with the changes within the H2A.Z when compared to the wildtype protein producing a more mobile structure(*72, 74*) with possibly similarly compact linker DNA. Although the mechanisms of this have not been worked out, it does to some degree concur with the results of the same assays used here on an acidic patch neutralized array type, described in the following paragraph(*72, 74*).

In terms of H2A.Z mechanism on chromatin structure, it's worth noting that another member of the lab where this thesis was performed, Charles "CJ" McDonald, recently constructed nucleosomal arrays where H2A's acidic patch amino acid residues were neutralized(*72*). Identical experiments were performed on these acidic patch mutant arrays as those completed in this thesis, including at the same time when H2A.Z and wildtype FRAP data was obtained (FRAP recovery curve in **Figure 20**) (*72, 74*). Compared to the wildtype arrays, FRAP on these arrays according to current results produced a lower overall mobile fraction of less than 20%, a decreased fast-recovering population composing 6.3% of the

mobile fraction, and a greater slow recovering population with 93.6% of the mobile fraction's constituents(*72, 74*). Although the half-lives were greater than the wildtype control arrays', they were less than that of the H2A.Z arrays(*72, 74*). The acidic patch mutant and H2A.Z array results construct a possible hypothesis where the acidic patch is instrumental in the fluctuations of nucleosomal array oligomers, promoting a more euchromatic-type state. Furthermore, although acidic patch neutralized arrays produced no differential centrifugation assay difference than wildtype arrays, the oligomerized form was leas readably digested and thus less accessible to the micrococcal nuclease protein than the control(*72*). Thus, the differences seen in the extended acidic path of H2A.Z and that of wildtype arrays are likely related at least in part due to the acidic patch(*72*) and not purely that of H2A.Z's altering histone dimer-dimer and or dimer-tetramer relationship. Furthermore, charge likely plays a role in this difference although not necessarily in a strictly-columbic fashion based on acidic path mutant differential centrifugation data(*72*).

4.3: H2A Double Tailless Arrays Discussion

The magnesium-induced oligomerization curve of the H2A double tailless arrays was shifted to the right of the wildtype curve, where part of the wildtype curve was from a laboratory collaborator (**Figure 8**)(*72*). Thus, the tailless arrays required more magnesium than the wildtype arrays to pellet in the differential centrifugation assay, and thus increased divalent cation to oligomerize(*72*). In addition, the likely extended H2A tailless arrays in their 2.5mM NaCl low salt buffer produced a fifty-percent sedimentation value of approximately 31.5 S. This S value was higher than that of the wildtype arrays, which had a midpoint S value distribution of approximately 28-28.5 S(*72*). The increased S value in the H2A tailless arrays under a non oligomerized state possibly suggests that the H2A tailless arrays had an increased ratio of moles of histones per DNA sequence repeat, and thus increased amounts of histones compared to that of the wildtype arrays under the low monomeric salt condition(*72*). An array sample with increased amounts of net positively charged histones would likely require less magnesium to

oligomerize, which would shift the differential centrifugation curve to the left. Therefore, if the only difference between the wildtype and H2A tailless arrays was the difference in S values, the H2A tailless arrays would be predicted to require less magnesium to oligomerize in the differential centrifugation assay. This was not the case. As a result, it is hypothesized that the H2A tailless arrays actually require more magnesium to oligomerize than what the differential centrifugation assay results predicted, and that this likely additional shift of the H2A tailless magnesium-induced oligomerization curve to the left is mitigated when compared to that of the wildtype arrays(*72*) by the H2A tailless array type's increased histone: DNA ratio as predicted by the increased sedimentation value under low salt conditions.

While no known studies have tested the effect of the H2A C-terminal tail on oligomerization, elimination of only H2A's N-terminal tail shifted the Mg50 point to 3mM Mg from the wildtype Mg50 of 2mM Mg(*32*). In this current study, the Mg50 was 1-2mM (~1.5mM) for wildtype(*72*) and 2-3mM Mg (~2.5mM) for tailless H2A, a change similar in raw Mg50 number but moderately proportionally greater than that of the comparable 208-12 nucleosomal arrays study(*32, 72*). Thus, while some of this change could be attributed to the N terminal tail, it is possible that the H2A C terminal tail is influential as well. The H4 N terminal tail truncation shifted the Mg50 to between 4-6mM Mg(*72*), rendering the combinatorial effect of the H2A tails less than that of the H4 tail in this regard, in line with the H2A N terminal tail compared to the H3 and H4 tails but more important than the H2B tail (*32*). In the current study, a net of 7 positive charges were removed by the combination of removing both tails from one histone H2A protein in the tailless protein construct, and it is likely that the positive charge loss is the driving force of requiring increased magnesium to make up for this loss to achieve a coulombic state necessary for oligomerization. This suggests that the H2A N, C, or both terminal tails neutralize negative charge(s). This is likely to be linker DNA for the C terminal tail at least in lower salt concentrations as previously reviewed (*39*).

The H2A tailless arrays digested at a slightly slower rate by micrococcal nuclease compared to wildtype arrays, and thus had slightly less linker DNA accessibility (**Figures 16-17**), as analyzed in **Figure 18**. Thus, it is likely that the H2A tails have a limited role in administering linker DNA accessibility and can be mostly substituted in this regard by increased magnesium. The only other known use of this assay on tails at an in vivo and oligomerization relevant divalent cation concentration showed that H4 tail truncation produced a slower digestion rate, advocating that the H4 tail orchestrates more accessible linker DNA(*72*). Thus, the H2A tails likely have a different mechanism in array oligomerization than the H4 tail(*72*), despite both histones' tail(s) likely binding to a negatively charged surface.

It was hypothesized prior to the study that the H2A tailless construct would require increased magnesium to oligomerize when compared to the wildtype arrays, which held true(*72*). However, the micrococcal nuclease results produced a slight difference in digestion rate, and thus possibly marginally less accessible linker DNA accessibility according to the micrococcal nuclease assay. This contrasted with the prediction that the tailless arrays would have a faster digestion rate as they were thought to form a less compact state. The FRAP results of the H2A tailless arrays producing a less mobile structure has yet to be tested. Therefore, in contrast to the hypotheses, the H2A tailless arrays promoted a slightly more closed chromatin structure, and as a result the tails help construct a marginally more open oligomer. The methodology behind this is a work in progress, but it aligns with the idea that chromatin is liquid-like in nature at least in part as a result of the intrinsically disordered tails(*3, 69*).

In order to digest its linker DNA target, micrococcal nuclease enzyme must travel to and then bind to its target. A static, compact state would likely be most inaccessible to digestion, and an open fluid structure would be most welcoming. This balance is approximately equal between the wildtype and H2A tailless array types. From the differential centrifugation assay, it could be hypothesized that the H2A tail(s) bind to a negative charge, DNA being the most likely option. The intrinsically disordered positive-charged rich tails likely participate in tail-bridging(*88*), attracting distant DNA or negatively

charged protein sites to induce transient compaction at that location. Removal of all N terminal tails inhibits oligomerization(*32*). However, increased magnesium concentration compared to wildtype arrays was likely able to substitute to most extent for the H2A C and N terminal tails for the tailless H2A's oligomerized arrays slightly less accessible linker DNA. Magnesium can mask negative charges but magnesium is less likely than the tails to bridge two array components together. Therefore, it's possible that the tails bind to a DNA location that minimally decreases local or global compaction. The tails could also bind nucleosomal DNA or a DNA region that was already in close proximity as a result of the H4, H3, and or H2B tails' efforts. Alternatively, the H2A tails could increase fluidity and thus accessibility to the micrococcal nuclease while concurrently orchestrating a more compact state, or vice versa, such that the balance between these two leads to marginally more accessible linker DNA as with magnesium substituting for the tails. However, the tails are less probable to create a compact, static oligomerized state by their intrinsically disordered nature. Fluidity and compactness by definition are at odds, making this tradeoff view a less favorable hypothesis. Additionally, the H2A tails could play little or no role at all if their function is to bind the chloride counter-ions, although increased magnesium concentrations in this assay also increases chloride concentrations in the differential centrifugation assay rendering this less likely. Of these conceivable explanations, it is most plausible that the H2A tails bind DNA that was already in close contact to these relatively short histone tails, decreasing chromatin compaction to some extent, but further research is necessary to support this idea. Additional work is also necessary to construct a clearer picture of the H2A tails' potential role in processes including transcription, DNA repair and replication, and in chromatin remodeling. Performing FRAP on H2A tailless oligomers with a reliably functioning microscope, as well as sedimentation velocity analytical ultracentrifugation with interference optics on a functional AUC system, would provide further insight into the dynamics and structures of these oligomers. Based on the identical-to-wildtype micrococcal nuclease results, however,

the H2A tailless arrays were hypothesized to have similar recovery fractions and similar sedimentation values as their wildtype counterparts.

4.4: Future Experiments

Obtaining fluorescence recovery after photobleaching (FRAP) data on the H2A tailless arrays was one of the goals of this work but was cut short due to microscope malfunctions on multiple occasions. It would also be interesting to test the H2A.Z and H2A tailless arrays with interference optics-based sedimentation velocity analytical ultracentrifugation for further size and shape analysis. Other array types involving histone variants include MacroH2A and H2A.Bbd. As the linker histone H1 is found in vivo, adding this histone to H2A tailless and H2A.Z arrays would be intriguing. It is likely that future experiments in the lab will include analyzing the effects that the histone H3 N terminal tail has on chromosome structure through the deletion of this region. In addition, nucleosomal arrays with different linker DNA repeat lengths will also be tested. Furthermore, FRAP experiments on wildtype arrays with linker histone H1 will likely be done. Post-translational modifications, including methylation and acetylation, are important in modifying chromatin structure, and the in vitro assay used could potentially be subjected to these modifications as well. Since chromatin in living cells is a heterogeneous complex of different histone variants, modifications, non-histone proteins, and RNA, subjecting multitudes of these variants to controls using the in vitro method here could also be useful.

CHAPTER 5: CONCLUSIONS

The histones H2A and H2A.Z are influential in determining the overall nucleosomal array composed oligomer shape(*72, 74*) and possibly that of similar in vivo domains as well. The H2A.Z variant required increased magnesium to mask its extended negatively charged acidic patch to oligomerize(*72*), but this effect had minimal effect on its linker DNA accessibility once oligomerized. The final structure required no post-translational or chromatin remodeling complex help to grant admission to a protein enzyme. This structure expressed an increased mobile fraction compared to the H2A wildtype control oligomerized arrays(*72, 74*). It also displayed an increased and more mobile euchromatin indicative demographic than its canonical H2A, while its less mobile constituents displayed less fluctuation(*72, 74*). The acidic patch is likely instrumental in these differences(*72, 74*). Removal of the canonical H2A N and C terminal tails required increased magnesium to produced nucleosomal array oligomers(*72*) and slightly increased its oligomers' linker DNA accessibility. It is possible that these tails are contributors to higher order chromatin structure in neutralizing already local negative charges on DNA or proteins but are not the primary components in tail mediated interactions that drive structure and mobility. Overall, H2A and H2A.Z are instrumental to defining the chromatin structure whose variability is necessary to the survival of life.

REFERENCES

1. Sutton, W. S. (1903) The chromosomes in heredity, *Biological Bulletin 4*, 231-251.
2. Avery, O. T., MacLeod , C.M., and MacCarty, M. (1943) Studies on the chemical nature of the substance inducing the transformation of pneumococcal types, *The Rockefeller Institute for Medical Research 79*, 137-159.
3. Hansen, J. C., Connolly, M., McDonald, C. J., Pan, A., Pryamkova, A., Ray, K., Seidel, E., Tamura, S., Rogge, R., and Maeshima, K. (2017) The 10-nm chromatin fiber and its relationship to interphase chromosome organization, *Biochemical Society transactions 5*, BST20170101.
4. Maeshima, K., Rogge, R., Tamura, S., Joti, Y., Hikima, T., Szerlong, H., Krause, C., Herman, J., Seidel, E., DeLuca, J., Ishikawa, T., and Hansen, J. C. (2016) Nucleosomal arrays self-assemble into supramolecular globular structures lacking 30-nm fibers, *The EMBO journal 35*, 1115-1132.
5. Maeshima, K., Hihara, S., and Eltsov, M. (2010) Chromatin structure: does the 30-nm fibre exist in vivo?, *Current opinion in cell biology 22*, 291-297.
6. Maeshima, K., Imai, R., Tamura, S., and Nozaki, T. (2014) Chromatin as dynamic 10-nm fibers, *Chromosoma 123*, 225-237.
7. Nishino, Y., Eltsov, M., Joti, Y., Ito, K., Takata, H., Takahashi, Y., Hihara, S., Frangakis, A. S., Imamoto, N., Ishikawa, T., and Maeshima, K. (2012) Human mitotic chromosomes consist predominantly of irregularly folded nucleosome fibres without a 30-nm chromatin structure, *The EMBO journal 31*, 1644-1653.
8. Luger, K., Mader, A. W., Richmond, R. K., Sargent, D. F., and Richmond, T. J. (1997) Crystal structure of the nucleosome core particle at 2.8 A resolution, *Nature 389*, 251-260.
9. Cutter, A. R., and Hayes, J. J. (2015) A brief review of nucleosome structure, *FEBS letters 589*, 2914-2922.
10. Rogge, R. A., Kalashnikova, A. A., Muthurajan, U. M., Porter-Goff, M. E., Luger, K., and Hansen, J. C. (2013) Assembly of Nucleosomal Arrays from Recombinant Core Histones and Nucleosome Positioning DNA, *Journal of visualized experiments: JoVE*.
11. Hansen, J. C. (2002) Conformational dynamics of the chromatin fiber in solution: determinants, mechanisms, and functions, *Annual review of biophysics and biomolecular structure 31*, 361-392.
12. Kornberg, R. D., and Thomas, J. O. (1974) Chromatin structure; oligomers of the histones, *Science 184*, 865-868.
13. Grosberg, A. Y. (2012) How two meters of DNA fit into a cell nucleus: Polymer models with topological constraints and experimental data, *Polymer Science Series C 54*, 1-10.
14. Jeffrey C. Hansen, J. A., Valerie H. Stanik, and K. E. van Holde (1989) Homogeneous Reconstituted Oligonucleosomes, Evidence for Salt-Dependent Folding in the Absence of Histone H1, *Biochemistry 28*, 9129-9136.
15. Widom, J., and Klug, A. (1985) Structure of the 300A chromatin filament: X-ray diffraction from oriented samples, *Cell 43*, 207-213.
16. Woodcock, C. L., Frado, L. L., and Rattner, J. B. (1984) The higher-order structure of chromatin: evidence for a helical ribbon arrangement, *The Journal of cell biology 99*, 42-52.
17. Joti, Y., Hikima, T., Nishino, Y., Kamada, F., Hihara, S., Takata, H., Ishikawa, T., and Maeshima, K. (2012) Chromosomes without a 30-nm chromatin fiber, *Nucleus 3*, 404-410.
18. Strick, R., Strissel, P. L., Gavrilov, K., and Levi-Setti, R. (2001) Cation-chromatin binding as shown by ion microscopy is essential for the structural integrity of chromosomes, *The Journal of cell biology 155*, 899-910.

19. Schwarz, P. M., Felthauser, A., Fletcher, T. M., and Hansen, J. C. (1996) Reversible oligonucleosome self-association: dependence on divalent cations and core histone tail domains, *Biochemistry 35*, 4009-4015.
20. Ciabrelli, F., and Cavalli, G. (2015) Chromatin-driven behavior of topologically associating domains, *Journal of molecular biology 427*, 608-625.
21. Dixon, J. R., Gorkin, D. U., and Ren, B. (2016) Chromatin Domains: The Unit of Chromosome Organization, *Molecular cell 62*, 668-680.
22. Fudenberg, G., Imakaev, M., Lu, C., Goloborodko, A., Abdennur, N., and Mirny, L. A. (2016) Formation of Chromosomal Domains by Loop Extrusion, *Cell reports 15*, 2038-2049.
23. Lonfat, N., and Duboule, D. (2015) Structure, function and evolution of topologically associating domains (TADs) at HOX loci, *FEBS letters 589*, 2869-2876.
24. Dixon, J. R., Selvaraj, S., Yue, F., Kim, A., Li, Y., Shen, Y., Hu, M., Liu, J. S., and Ren, B. (2012) Topological domains in mammalian genomes identified by analysis of chromatin interactions, *Nature 485*, 376-380.
25. Gibcus, J. H., and Dekker, J. (2013) The hierarchy of the 3D genome, *Molecular cell 49*, 773-782.
26. Razin, S. V., Gavrilov, A. A., Kos, P., and Ulianov, S. V. (2017) Self-organization of a chromatin fibril into topologically-associated domains, *Russian Journal of Bioorganic Chemistry 43*, 99-106.
27. Schwarz P.M. and Hansen, J. C. (1994) Formation and stability of higher order chromatin structures, *Biochemistry 35*, 4009-4015.
28. Mathieson, A. R., and J.Y. Olayemi. . (1975) The interaction of calcium and magnesium ions with deoxyribonucleic acid, *Arch. Biochem. Biophys. 169*, 237–243.
29. Korolev, N., Allahverdi, A., Lyubartsev, A. P., and Nordenskiöld, L. (2012) The polyelectrolyte properties of chromatin, *Soft Matter 8*, 9322.
30. de Frutos, M., Raspaud, E., Leforestier, A., and Livolant, F. (2001) Aggregation of nucleosomes by divalent cations, *Biophysical journal 81*, 1127-1132.
31. Bloomfield, V. A. (1998) DNA condensation by multivalent cations, *Biopolymers 44*, 269-282.
32. Gordon, F., Luger, K., and Hansen, J. C. (2005) The core histone N-terminal tail domains function independently and additively during salt-dependent oligomerization of nucleosomal arrays, *The Journal of biological chemistry 280*, 33701-33706.
33. Arya, G. a. S., T. (2009) A tail of tails: how they mediate chromatin compaction in different salt and linker histone environments, *Journal of Physical Chemistry*, 4045-4059.
34. Bloomfield, I. R. a. V. A. (1998) DNA bending by small, mobile multivalent cations, *Biophysical journal 74*, 3152-3164.
35. Hansen, T. M. F. a. J. C. (1995) Core histone tail domains mediate oligonucleosome folding and nucleosomal DNA organization through distinct molecular mechanisms, *The Journal of biological chemistry 270*, 25359-25362.
36. Korolev, N., Allahverdi, A., Yang, Y., Fan, Y., Lyubartsev, A. P., and Nordenskiold, L. (2010) Electrostatic origin of salt-induced nucleosome array compaction, *Biophysical journal 99*, 1896-1905.
37. Bertin, A., Leforestier, A., Durand, D., and Livolant, F. (2004) Role of histone tails in conformation and interactions of nucleosome core particles, *Biochemistry 43*, 4773-4780.
38. Hansen, J. C., Tse, C., and Wolffe, A.P. . (1998) Structure and function of the core histone N-termini: more than meets the eye, *American Chemical 37*, 17637-17641.
39. Zheng, C., and Hayes, J.J. (2002) Structures and Interactions of the Core Histone Tail Domains, *Biopolymers 68*, 539-546.
40. Hayes, K.-M. L. a. J. J. (1998) Linker DNA and H1-Dependent Reorganization of Histone-DNA Interactions within the Nucleosome, *Biochemistry 37*, 8622-8628.

41. Erler, J., Zhang, R., Petridis, L., Cheng, X., Smith, J. C., and Langowski, J. (2014) The role of histone tails in the nucleosome: a computational study, *Biophysical journal 107*, 2911-2922.
42. Vogler, C., Huber, C., Waldmann, T., Ettig, R., Braun, L., Izzo, A., Daujat, S., Chassignet, I., Lopez-Contreras, A. J., Fernandez-Capetillo, O., Dundr, M., Rippe, K., Langst, G., and Schneider, R. (2010) Histone H2A C-terminus regulates chromatin dynamics, remodeling, and histone H1 binding, *PLoS genetics 6*, e1001234.
43. West, M. H. a. B., W. M. (1980) Histone 2A, a Heteromorphous Family of Eight Protein Species, *Biochemistry 19*, 3238-3245.
44. Millar, C. B. (2013) Organizing the genome with H2A histone variants, *The Biochemical journal 449*, 567-579.
45. Chakravarthy, S., Gundimella, S. K., Caron, C., Perche, P. Y., Pehrson, J. R., Khochbin, S., and Luger, K. (2005) Structural characterization of the histone variant macroH2A, *Molecular and cellular biology 25*, 7616-7624.
46. Suto, R. K., Clarkson, M.J., Tremethick, D.J., and Luger, K. (2000) Crystal structure of a nucleosome core particle containing the variant histone H2A.Z, *Nature structural biology 7*, 1121-1124.
47. Kalashnikova, A. A., Porter-Goff, M. E., Muthurajan, U. M., Luger, K., and Hansen, J. C. (2013) The role of the nucleosome acidic patch in modulating higher order chromatin structure, *Journal of the Royal Society, Interface 10*, 20121022.
48. Barbera AJ, C. J., Kelley-Clarke B, Joukov V, Walter JC, Luger K, Kaye KM. (2006) The nucleosomal surface as a docking station for Kaposi's sarcoma herpesvirus LANA., *Science 311*, 856–861.
49. Roussel L, E. M., Cayrol C, Girard J-P. (2008) Molecular mimicry between IL-33 and KSHV for attachment to chromatin through the H2A-H2B acidic pocket, *EMBO Rep 9*, 1006–1012.
50. Fan, J. Y., Rangasamy, D., Luger, K., and Tremethick, D. J. (2004) H2A.Z alters the nucleosome surface to promote HP1alpha-mediated chromatin fiber folding, *Molecular cell 16*, 655-661.
51. Faast, R., Thonglairoam, V., Schulz, T.C., Beall, J., Wells, J.R., Taylor, H., Matthaei, K., Rathjen, P.D., Tremethick, D.J., and Lyons, I. (2001) Histone variant H2A.Z is required for early mammalian development, *Curr. Biol. 11*, 1183–1187.
52. Lu, A., Steege, A., and Stafford, D.W. (1980) Nucleotide sequence of a 5S ribosomal RNA gene in the sea urchin Lytechinus variegatus, *Nucleic acids research 8*, 1839-1853.
53. Lohr, J. C. H. a. D. (1993) Assembly and Structural Properties of Subsaturated Chromatin Arrays, *288*, 5840-5848.
54. Thastrom, A., Lowary, P.T., Widlund, H.R., Cao, H., Kubista, M., and Widom, J. (1999) Sequence motifs and free energies of selected natural and non-natural nucleosome postioning DNA sequences, *Journal of molecular biology 288*, 213-229.
55. Prunell, A. (1977) Relation of Nucleosomes to DNA Sequences, *Cold Spring Harbor Symposia on Quantitative Biology 42*, 103-108.
56. Telford, D. J. a. S., B.W. . (1988) Micrococcal nuclease: its specificity and use for chromatin analysis, *International Journal of Biochemistry 21*, 127-137.
57. Dong, F., Hansen, J.C., and van Holde, K.E. (1990) DNA and protein determinants of nucleosome positioning on sea urchin 5S rRNA gene sequences in vitro, *National Academy of Sciences 87*, 5724-5728.
58. Visvanathan, A., Ahmed, K., Even-Faitelson, L., Lleres, D., Bazett-Jones, D. P., and Lamond, A. I. (2013) Modulation of Higher Order Chromatin Conformation in Mammalian Cell Nuclei Can Be Mediated by Polyamines and Divalent Cations, *PloS one 8*, e67689.
59. Garcia-Ramirez, M., Dong, F., and Ausio, J. (1992) Role of the histone tail in the folding of oligonucleosomes depleted of histone H1, *The Journal of biological chemistry 267*, 19587-19595.

60. Hansen, J. C., Lebowitz, J., and Demeler, B. (1994) Analytical ultracentrifugation of complex macromolecular systems, *Biochemistry 33*, 13155-13163.
61. Rogge, R. A., and Hansen, J. C. (2015) Sedimentation Velocity Analysis of Large Oligomeric Chromatin Complexes Using Interference Detection, *Methods in enzymology 562*, 349-362.
62. Noll, M. (1977) Action of Micrococcal Nuclease on Chromatin and Locatoin of Histone H-1, *Journal of molecular biology 109*, 393-404.
63. Cunningham, L., Catlin, W., and De Garilhe, P. (1956) A Deoxyribonuclease of Micrococcus pyogenes, *Journal of the American Chemical Society 78*, 4643-4645.
64. Dingwall, C., Lomonossoff, G.P., and Laskey, R.A. (1981) High sequence specificity of micrococcal nuclease, *Nucleic acids research 9*, 2659-2673.
65. Cockell, M., Rhodes, D., and Klug, A. (1983) Locations of the primary sites of micrococcal nuclease cleavage on the nucleosome core, *Journal of molecular biology 170*, 423-446.
66. Ishikawa-Ankerhold, H. C., Ankerhold, R., and Drummen, G. P. (2012) Advanced fluorescence microscopy techniques--FRAP, FLIP, FLAP, FRET and FLIM, *Molecules 17*, 4047-4132.
67. Zipper, H., Brunner, H., Bernhagen, J., and Vitzthum, F. (2004) Investigations on DNA intercalation and surface binding by SYBR Green I, its structure determination and methodological implications, *Nucleic acids research 32*, e103.
68. Dragan, A. I., Pavlovic, R., McGivney, J. B., Casas-Finet, J. R., Bishop, E. S., Strouse, R. J., Schenerman, M. A., and Geddes, C. D. (2012) SYBR Green I: fluorescence properties and interaction with DNA, *Journal of fluorescence 22*, 1189-1199.
69. Maeshima, K., Ide, S., Hibino, K., and Sasai, M. (2016) Liquid-like behavior of chromatin, *Current opinion in genetics & development 37*, 36-45.
70. Saera Hihara, C.-G. P., Kazunari Kaizu, Tomomi Tani, Tomo Hanafusa, Tadasu Nozaki,, Satoko Takemoto, T. Y., Hideo Yokota, Naoko Imamoto, Yasushi Sako, Masataka Kinjo,, and Koichi Takahashi, T. N., and Kazuhiro Maeshima. (2012) Local Nucleosome Dynamics Facilitate Chromatin Accessibility in Living Mammalian Cells, *Cell reports 2*, 1645-1656.
71. Hansen, J. C. a. v. H., K.E. (1991) The Mechanism of Nucleosome Assembly onto Oligomers of the Sea Urchin 5 S DNA Positioning Sequence, *The Journal of biological chemistry 266*, 4276-4282.
72. McDonald, C. J. (2017) Role of the H4 N-terminal tail and nucleosome acidic patch in chromatin oligomer dynamics, In *Deparment of Biochemistry and Molecular Biology*, Colorado State University, Fort Collins, CO.
73. McDonald, C. J. (2016) Unpublished Work: Wildtype Octamer and Wildtype Nucleosomal Array Construction, Colorado State University, Fort Collins, CO.
74. Connolly M. and McDonald, C. J. (2017) Unpublished Work: FRAP Data and Images, Colorado State University, Fort Collins, CO.
75. Brunelle, M., Nordell Markovits, A., Rodrigue, S., Lupien, M., Jacques, P. E., and Gevry, N. (2015) The histone variant H2A.Z is an important regulator of enhancer activity, *Nucleic acids research 43*, 9742-9756.
76. Chen, Q., Yang, R., Korolev, N., Liu, C. F., and Nordenskiold, L. (2017) Regulation of Nucleosome Stacking and Chromatin Compaction by the Histone H4 N-Terminal Tail-H2A Acidic Patch Interaction, *Journal of molecular biology 429*, 2075-2092.
77. Chodaparambil, J. V., Barbera, A. J., Lu, X., Kaye, K. M., Hansen, J. C., and Luger, K. (2007) A charged and contoured surface on the nucleosome regulates chromatin compaction, *Nature structural & molecular biology 14*, 1105-1107.
78. Christin Tse, T. S., Alan P. Wolffe, and Jeffrey C. Hansen. (1998) Disruption of Higher-Order Folding by Core Histone Acetylation Dramatically Enhances Transcription of Nucleosomal Arrays by RNA Polymerase III, *Molecular and cellular biology 18*, 4629-4638.

79. Sinha, D., and Shogren-Knaak, M. A. (2010) Role of direct interactions between the histone H4 Tail and the H2A core in long range nucleosome contacts, *The Journal of biological chemistry 285*, 16572-16581.
80. Fan, J. Y., Gordon, F., Luger, K., Hansen, J. C., and Tremethick, D. J. (2002) The essential histone variant H2A.Z regulates the equilibrium between different chromatin conformational states, *Nature structural biology 9*, 172-176.
81. Bonisch, C., and Hake, S. B. (2012) Histone H2A variants in nucleosomes and chromatin: more or less stable?, *Nucleic acids research 40*, 10719-10741.
82. Hardy, S., Jacques, P. E., Gevry, N., Forest, A., Fortin, M. E., Laflamme, L., Gaudreau, L., and Robert, F. (2009) The euchromatic and heterochromatic landscapes are shaped by antagonizing effects of transcription on H2A.Z deposition, *PLoS genetics 5*, e1000687.
83. Nozaki, T., Imai, R., Tanbo, M., Nagashima, R., Tamura, S., Tani, T., Joti, Y., Tomita, M., Hibino, K., Kanemaki, M. T., Wendt, K. S., Okada, Y., Nagai, T., and Maeshima, K. (2017) Dynamic Organization of Chromatin Domains Revealed by Super-Resolution Live-Cell Imaging, *Molecular cell 67*, 282-293 e287.
84. Pugh, Z. Z. a. B. F. (2011) Genomic Organization of H2Av Containing Nucleosomes in Drosophila Heterochromatin, *PloS one 6*, e20511.
85. Guillemette B, B. A., Gévry N, Adam M, Blanchette M, Robert F, and Gaudreau L. (2005) Variant histone H2A.Z is globally localized to the promoters of inactive yeast genes and regulates nucleosome positioning, *PLoS Biology 12*, e384.
86. Rangasamy, D., Breven, L., Ridgway, P., and Tremethick, D.J. (2003) Pericentric heterochromatin becomes enriched with H2A.Z during early mammalian development, *The EMBO journal 22*, 1599-1607.
87. Takata, H., Hanafusa, T., Mori, T., Shimura, M., Iida, Y., Ishikawa, K., Yoshikawa, K., Yoshikawa, Y., and Maeshima, K. (2013) Chromatin compaction protects genomic DNA from radiation damage, *PloS one 8*, e75622.
88. Mühlbacher, F., Holm, C., and Schiessel, H. (2006) Controlled DNA compaction within chromatin: The tail-bridging effect, *Europhysics Letters (EPL) 73*, 135-141.